aptara | GJI | gji_4107 | Dispatch: March 4, 2009 | CE:
Journal | MSP No. | No. of pages: 24 | PE: Gregor

Geophys. J. Int. (2009) doi: 10.1111/j.1365-246X.2009.04107.x

Seismotectonics in Northeast India: a stress analysis of focal mechanism solutions of earthquakes and its kinematic implications

Jacques Angelier[1,2] and Saurabh Baruah[3]

[1] *Observatoire Océanologique de Villefranche (UPMC), Géosciences Azur,* B.P.48, *La Darse,* 06235 *Villefranche-sur-Mer, France*
[2] *Institut Universitaire de France, France. E-mail: jacques.angelier@geoazur.obs-vlfr.fr*
[3] *Geoscience Division, North-East Institute of Science and Technology (formerly Regional Research Laboratory), under Council of Scientific and Industrial Research, Jorhat* 785006, *Assam, India*

Accepted 2009 January 5. Received 2008 December 12; in original form 2008 July 10

SUMMARY

In Northeast India, three major plates interact along two convergent boundaries: the Himalayas and the Indo–Burma Ranges, which meet at the Assam Syntaxis. To clarify this tectonic interaction and the underlying dynamics, we determine the regional seismotectonic stress from the stress inversion of 285 double couple focal mechanism solutions of earthquakes with an average magnitude of 5. We then compare the reconstructed stress regimes with the available information about geodetically determined relative displacements.

North–south compression, in a direction consistent with India–Eurasia convergence, prevails in the whole area from the Eastern Himalayas to the Bengal Basin, through the Shillong–Mikir Massif and the Upper Assam Valley. E–W extension in Tibet is related to this N–S India–Eurasia convergence. Not only does the major N–S compression affect the outer segments of the Indo–Burma Ranges, it also extends into the descending slab of Indian lithosphere below these Iranges, although stresses at depth are controlled by bending of the slab beneath the Burmese arc.

The existence of widespread N–S compression in the Bengal Basin, far away from the Himalayan front, is compatible with the previously proposed convergence between a Shillong–Mikir–Assam Valley block and the Indian craton. E–W compression inside this block supports the hypothesis of a component of eastward extrusion.

Stress inversion of focal mechanism solutions in the Indo–Burma Ranges reveals a complex stress pattern. The Burmese arc and its underlying lithosphere experience nearly arc-perpendicular extension with ESE–WNW trends in the northernmost, NE-trending segment and ENE–WSW trends in the main N–S arc segment. Such extensional stress, documented from many arcs, is likely a response to pull from and bending of the subducting plate.

At the same time, the Indo–Burma Ranges are under compression as a result of oblique convergence between the Sunda and Indian plates. The maximum compressive stress rotates from NE–SW across the inner and northern arc to E–W near the Bengal Basin. This rotation is consistent with the deformation partitioning reflected in the rotation of relative displacement vectors, from a SSW-directed Sunda–Burma motion to a WSW-directed Burma–India motion. As a consequence of this partitioning, the major belt-parallel fault zones show a variety of movements across the main N–S arc segment, from right-lateral slip in the inner ranges to oblique reverse-dextral slip in the outer ranges and pure thrusting in the westernmost foreland belt.

Key words: ???.

1 INTRODUCTION

In Northeast India and its adjacent regions, convergence occurs between three major plates—India, Eurasia and Sunda. The domain between 20°N–31°N in latitude and 86°E–98°E in longitude (Fig. 1) thus includes two major mountain ranges—the Eastern Himalayas to the north and the Indo–Burma Ranges to the southeast, in addition to a large intraplate domain of India.

Although there is a general agreement regarding the existence of N–S compression related to plate convergence between India and

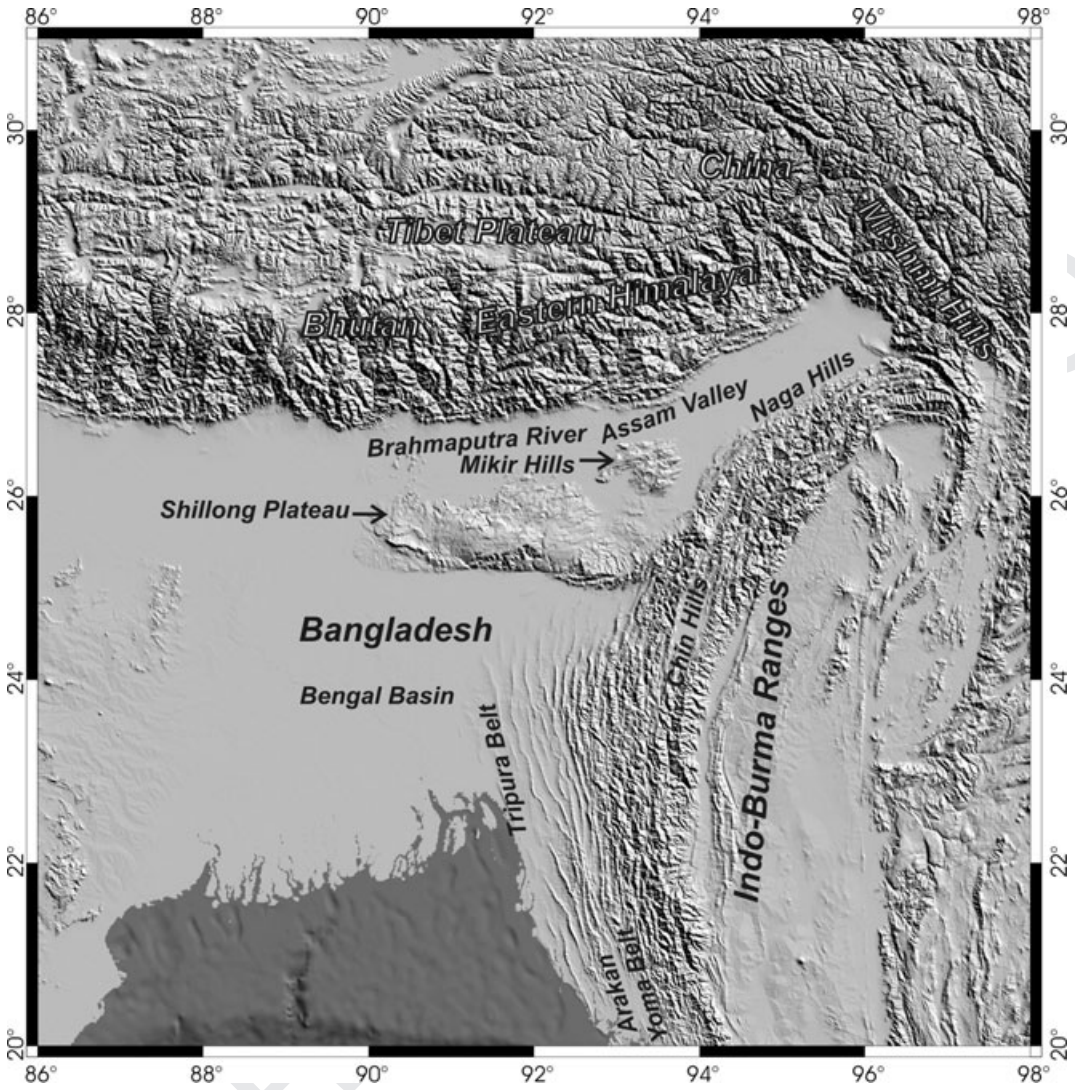

Figure 1. Shaded relief map of Northeast India and surrounding regions. The main regional morphological units are named. The major structural units are presented in Fig. 2.

Eurasia, the variations in the direction of compression and even the type and orientations of seismotectonic stress regimes are poorly known, especially in the Indo–Burma Ranges and in the Assam syntaxis, where the two major mountain belts meet near 28°N and 96°E. The inversion of focal mechanisms solutions of earthquakes to determine the seismotectonic stress regimes done in this paper provides a new way to decipher the active tectonics of the area and to evaluate the geodynamic implications, additionally, taking into account the recent kinematic information from geodetic studies.

The E–W to ENE–WSW trending Eastern Himalaya collision belt north of 27°N (Fig. 2) includes south and southeast of the Tibet Plateau, the south-verging Main Central Thrust (MCT) and Main Boundary Thrust (MBT). The Indian plate is gently dipping to the north beneath the Himalayas (Zhao *et al.* 1993; Mitra *et al.* 2005). Many studies highlighted the role of continental collision (e.g. Le Fort 1975; Molnar & Tapponnier 1975; Tapponnier *et al.* 1986). The present-day compression is approximately N–S, as indicated by focal mechanism solutions and analyses of borehole breakouts (Gowd *et al.* 1992; Heidbach *et al.* 2005, 2007). N–S shortening is revealed by geodetic studies (Bilham & Gaur 2000; Jouanne *et al.* 2004; Jade *et al.* 2007).

South of 27°N and east of 93°E, in the Indo–Burma Ranges and subduction zone (Fig. 2), the Indian lithosphere is plunging eastwards below the Burmese arc, a fold-and-thrust belt with west-verging thrusts (Mukhopadhyay & Dasgupta 1988; Ni *et al.* 1989; Rai *et al.* 1996; Das Gupta *et al.* 2003; Khan 2005). This belt trends NNW–SSE to the south (the Arakan Yoma belt), N–S east of Bangladesh (the Chin Hills) and NE–SW to the north (the Naga Hills). Within this active tectonic framework (Le Dain *et al.* 1984), recent studies highlighted the kinematics of the Indian, Burmese and western Sunda plates (Socquet *et al.* 2006; Gahalaut & Gahalaut 2007). Variable amounts of thrusting and right-lateral slip affect the N–S trending structures of the western Burmese arc (Maung 1987; Vigny *et al.* 2003; Kayal *et al.* 2004), suggesting E–W and NE–SW compressions (Verma *et al.* 1976; Chandra 1984; Gowd *et al.* 1992; Ravikumar *et al.* 1996; Heidbach *et al.* 2005, 2007). However, the GPS stations revealing the present-day displacement pattern are still few (Jade *et al.* 2007), and major uncertainties exist regarding the seismotectonic stress regimes in and beneath the Burmese arc.

Near 28°N and 96°E, in the Assam syntaxis zone, the MBT units of the easternmost Himalayas and the Belt of Schuppen and Naga Thrust of the northernmost Burmese arc run parallel with

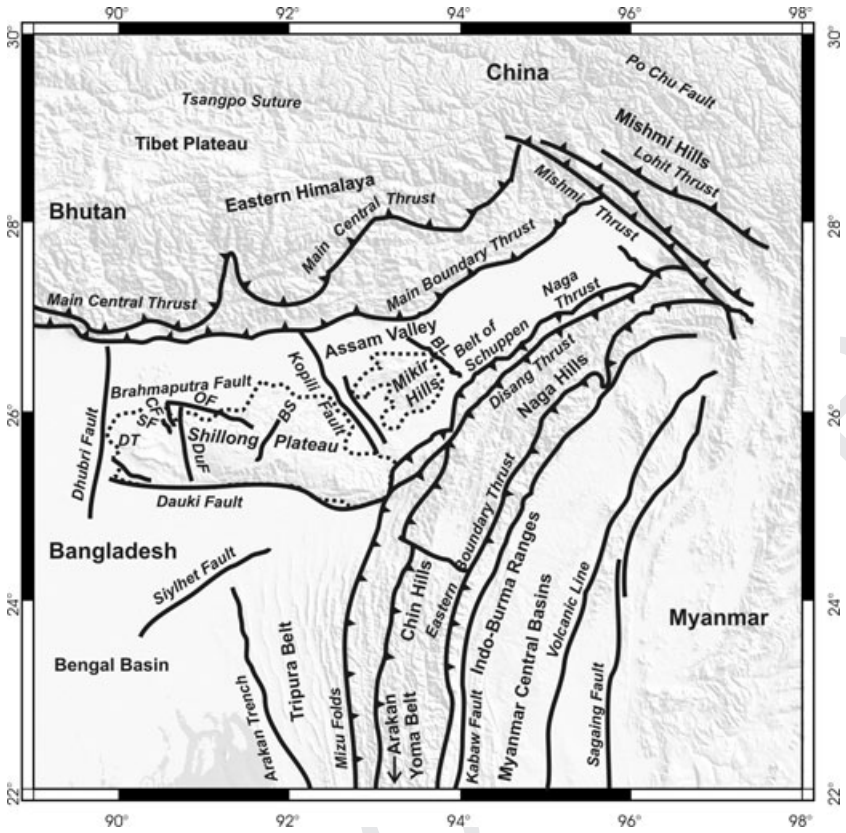

Figure 2. Tectonic setting of Northeast India and surrounding regions (adapted from Nandy 2001; also Murthy *et al.* 1969 and Kayal 1998). Major thrusts as thick lines with triangles on the upthrust side. Other major faults as simple thick lines. Boundaries of Shillong and Mikir plateaus are presented as dotted lines. Geological names in italic, geographic names in roman characters. Names of main faults and thrusts indicated, with some abbreviations in the western Shillong Plateau (DT, Dapsi Thrust; DuF, Dudhnoi Fault; OF, Oldham Fault; CF, Chedrang Fault; SF, Samin Fault, BS, Barapani Shear Zone) and eastern Mikir Plateau (BL, Bomdila Lineament).

ENE–WSW trends, on both sides of the upper Assam Valley (Fig. 2). This northeast portion of the Indian plate is bounded by major, all India-verging, thrust zones (MBT–MCT to the north, Lohit–Mishmi thrusts to the northeast, Naga, Disang and Eastern Boundary thrusts to the east, front thrusts of the Arakan Yoma Belt to the southeast). This intraplate domain is deformed in the Shillong Plateau and the Mikir Hills near 25°N–26°N and in the Tripura folded belt near 92°E–93°E (Figs 1 and 2). The converging structures forming a complicated geotectonic system (Curray *et al.* 1979, 1982; Nandy 2001) force the northeastern portion of the India plate to be deformed (Evans 1964; Chen & Molnar 1990; Kayal 1991; Rao & Kumar 1997; Bilham & England 2001). This region is seismically active (Das Gupta & Nandy 1982; Gupta *et al.* 1984; Kayal & De Reena 1991; Baruah *et al.* 1997; Kayal 1998; Rajendran *et al.* 2004; Bilham 2006; Kayal *et al.* 2006; Thingbaijam *et al.* 2008), with the remarkable exception of the Assam Gap (Khattri *et al.* 1983). For 200 yr, the whole region experienced 20 large earthquakes with magnitudes 7 or larger. Two very large earthquakes occurred on 1897 June 12 ($M \geq 8.5$; Oldham 1899) and 1950 August 15 ($M = 8.7$; Poddar 1950; Tillottson 1953). Various trends of compression have been suggested in this intraplate domain (Gowd *et al.* 1992; Heidbach *et al.* 2005, 2007; Baruah *et al.* 2007). However, non-consensus exists regarding the existence of a separate Shillong–Mikir–Assam Valley block and its possible motion with respect to India.

In this paper, we aim at solving these ambiguities and interpreting the active deformation in Northeast India through systematic determination of seismotectonic stress based on inversion of earthquake focal mechanism solutions. We show that despite the large extent and structural complexity of the studied region, it is possible to reconstruct consistent seismotectonic stress states, which are multiple in space and time. A reliable stress determination requires preliminary delineation of major structural domains and subregions, as well as consideration of depth where subduction occurs. We thus intend to clarify the geodynamic interaction between plates, especially regarding (1) the extent and azimuthal variations of N–S compression related to India–Eurasia convergence and (2) the geodynamic significance of seismotectonic mechanisms related to the subduction of Indian plate beneath Burmese arc, and their relation to kinematics. We finally intend to better characterise intraplate deformation in Northeast India.

2 TECTONIC SETTINGS

As converging plate boundary zones, the most deformed domains of the studied region are the Eastern Himalayas to the north and the Indo–Burma Ranges to the southeast. These two major mountain belts merge in the upper Assam Valley, forming the Assam Syntaxis. Between these two boundaries, a portion of the Indian Plate includes the Assam Valley and the Shillong and Mikir Plateaus (Fig. 2). Most of the Bangladesh area is occupied by the large Bengal Basin, with two main structural units separated by a Hinge Zone that trends NE–SW from Calcutta toward the Naga Hills in Assam. Whereas to the northwest, a platform environment prevails in the Indian

craton, to the southeast, the basement of the Indian plate gently dips towards the Bay of Bengal and the thickness of post-Mesozoic sediments increases, forming the Bengal foredeep at the western front of the Indo–Burma Ranges as a northern termination of the Arakan Trench.

2.1 Eastern Himalayas

The Himalaya is the largest orogenic belt of the world, where a continental crust underthrusts another continental crust (Zhao *et al.* 1993; Nandy 2001). The entire Himalayan arc evolved as a consequence of collision of the Asian and Indian continents about 50 Ma (Gansser 1964; McKenzie & Sclater 1971; Molnar & Tapponnier 1975; Mitchell 1981; Curray *et al.* 1982; Tapponnier *et al.* 1982, 1986). In the broad sense, the Arunachal Himalaya occupies the easternmost segment of the Himalaya between longitudes 91°30′E and 96°E and includes the eastern Himalayan syntaxis.

The MCT and MBT are the two major tectonic features in Eastern Himalaya (Fig. 2). The MCT is a major intracontinental ductile shear zone with an associated inverted metamorphic zone, which appears to have developed since mid-Tertiary time and also shows minor recent movements (Valdiya 1980). The MCT separates two geologically distinct zones—the Lesser Himalaya to the south and the Higher Himalayan Crystallines to the north. The main discontinuity between the sub-Himalayan and lesser Himalaya zones is the MBT, presently marked by intense seismicity and disastrous earthquakes. This major thrust zone developed since the Pliocene time and was active during the Pleistocene (Mathur & Evans 1964; Le Fort 1975; Valdiya 1980). West of the studied area, the sub-Himalayan zone shows a typical tectonic wedge of synorogenic sediments, incorporated into the prism of the foreland Indian basin along the front of the Himalayan belt (Husson *et al.* 2004).

Present-day slip occurs through large magnitude earthquakes along the gently north-dipping detachment zone of the MBT, with the front thrust as the lowest emergent ramp. Whereas satellite geodesy studies since 1995 indicated rates of N–S convergence in the range 10–15 mm yr^{-1} between the Indian craton and Himalayas, in western Nepal, a major seismic gap along this zone suggests locking rather than aseismic slip (Jouanne *et al.* 2004). In the easternmost Himalayas, the Assam syntaxis zone, where the Himalayan arc and the Burmese arc meet the Mishmi block, is an important tectonic domain with NW–SE thrust trends, such as for the Lohit and Mishmi thrusts (Fig. 2). This zone was the source area of the 1950 great earthquake (Poddar 1950).

2.2 Indo–Burman orogen

The other major mountain belt of the studied area is the Indo–Burman orogen, including Indo–Burma Ranges and Central Myanmar Basins (Fig. 2). Active faults are numerous in the Burma region (Le Dain *et al.* 1984). Convergence and subduction of the Indian plate occur along the Indo–Burma arc (Mitchell & Mckerrow 1975; Mitchell 1981). A slab of the Indian plate dips eastwards below the Burmese arc (Das & Filson 1975; Mukhopadhyay & Das Gupta 1988; Rai *et al.* 1996; Ravikumar *et al.* 1996; Satyabala 1998). Near 24°N–25°N, Khan (2005) reconstructed a dip of 24°–26° of the Wadati–Benioff surface across the Indo–Burma Ranges.

The subduction of the Indian lithosphere beneath Burma was regarded active (Verma *et al.* 1976; Chandra 1984, Mukhopadhyay & Dasgupta 1988; Satyabala 1998; Dasgupta *et al.* 2003), slow (Le Dain *et al.* 1984; Ni *et al.* 1989; Chen & Molnar 1990) or inactive (Rao & Kumar 1999). Based on 11 yr of GPS geodetic surveys, Socquet *et al.* (2006) determined the present-day rotation of the Sunda plate, revealing at the latitude of Myanmar a velocity of 35 mm yr^{-1} in the N10°E direction for India with respect to Sunda. These authors also showed that near 22°N the motion of India relative to Sunda is distributed across several major boundaries or deformation zones, including from east to west 18 mm yr^{-1} (toward N) along the Sagaing Fault, 9 mm yr^{-1} (toward NE) in Myanmar Central Basins and 14 mm yr^{-1} (also toward NE) absorbed across the western Indo–Burma Ranges and the Tripura belt. This velocity distribution is consistent with earlier interpretations in terms of decoupling and dextral transpression between the Indo–Burma Ranges and the underlying Indian plate (Maung 1987, Kayal *et al.* 2004).

The Indo–Burma Ranges are believed to have developed during the Oligocene time as a result of an eastward subduction (Brunnschweiler 1966). The major units in these ranges are composed of thick turbiditic sequences of Cretaceous to Upper Eocene age. From north to south, the structural trends change from NE–SW in the Naga Hills to N–S and even NNW–SSE along the Arakan-Yoma and Chin Hills (Fig. 2). East of the Eastern Boundary Thrust, a 200 km wide and 1400 km long Palaeogene and Neogene sedimentary basin is present in Central Myanmar. This basin is bounded by the major, N–S trending right-lateral Sagaing Fault to the east. At the front of the Indo–Burma Ranges, the eastern Tripura (or Tripura–Chittacong) fold system is a typical fold-and-thrust belt with west-verging thrusts as a result of the eastward subduction of the Indian Plate. Toward the west across the Tripura belt, where fan-shaped series of folds have clear morphological expression (Fig. 1), large belt-parallel folds and thrusts decrease in number toward the non-deformed foreland of the Bengal Basin.

2.3 Assam valley

The Assam Valley is an ENE–WSW trending, relatively narrow valley, bounded by two mobile young mountain belts to the north and southeast. The distance between the Himalayan Front (MBT) and the front of the Indo–Burma Ranges (Naga Thrust) is 100–110 km in the upper Assam Valley between 94°E and 96°E (Fig. 1). To the northeast, this zone is bounded by the SW-verging thrusts of the Mishmi block. To the west, between 90°E and 94°E, the Assam Valley Region is limited on the southern side by the Shillong and Mikir plateaus. The Brahmaputra River flows westwards along the Brahmaputra lineament, from Upper Assam to the Dhubri Fault, along which it flows to the south (Nandy & Das Gupta 1986).

The Archaean crystalline basement is overlain by Tertiary and Recent sediments, about 5 km thick in Upper Assam and thinning out downstream toward the Mikir Hills (Nandy 2001). The NNW–SSE Kopili Fault (Das Gupta & Nandy 1982) is a transverse fault zone crossing the Assam Valley between the Shillong and Mikir plateaus, from the MBT on the Himalayan side to the Belt of Schuppen on the Indo–Burman side (Fig. 2). The Belt of Schuppen has been defined by Mathur & Evans (1964) as a narrow linear belt of imbricate thrust slices, closely linked with the shortening and uplift of the Indo–Burma belt. In Lower Assam, the N–S Dhubri Fault bounds the Shillong Plateau to the west. The valley is covered with thick alluvium with few inselbergs of basement rocks (Nandy 2001). Almost flat-lying Tertiary shelf sediments overlie the basement with increasing thickness toward the Himalaya.

The entire Assam Valley shows low-level seismicity compared with other regions of Northeast India. The upper Assam Valley

from 92°E to 96°E, between the Kopili Fault and the Mishmi Thrust (Fig. 2), is almost free from seismic activity. This region was named 'Assam Gap' by Khattri *et al.* (1983).

2.4 Shillong–Mikir Plateaus

The Shillong Plateau in Northeast India (Fig. 1) is a part of the Indian Plate that was uplifted during the Latest Cenozoic (Rao & Kumar 1997). The Shillong Plateau and Mikir Hills consist of crystalline rocks partly covered by gently dipping Tertiary and younger sediments (Evans 1964; Kayal 1991). According to Evans (1964), this massif has been separated from the peninsular shield and moved to the east along the Dauki Fault. This E–W trending Dauki Fault (Murthy *et al.* 1969) separates the Shillong Plateau to the north and the Bengal Basin to the south. Regardless of the possible lateral component, the recent Dauki Fault is reverse and affects the Plio-Pleistocene piedmont sediments. To the north, along the Brahmaputra River valley, the main E–W trending northern boundary of the Shillong Plateau is the Brahmaputra Fault (Das Gupta & Nandy 1992). The graben structure of the NW–SE trending Kopili lineament separates the Shillong Plateau and its submassif, the Mikir Plateau (Nandy 2001). Two major thrust faults are present inside the Shillong Plateau, namely the Dapsi Thrust and the Barapani Shear Zone (Kayal 1991). The most important structures in this region are the E–W trending Brahmaputra and Dauki faults that bound the Shillong Plateau to the north and south, respectively, as well as a variety of N–S to NW–SE trending transverse faults (Fig. 2). All these structures developed between the nearly E–W trending MBT and the NE–SW trending Naga Thrust on the Himalayan and Indo–Burman sides, respectively.

The seismotectonic activity of the area was highlighted by the Great Assam earthquake in 1897. The maximum intensity affected the Chedrang Valley area (Oldham 1899). Uplift took place east of the Chedrang Fault, resulting in the formation of a lake on the west side. Oldham (1899) observed 11 m of coseismic offset. A south-dipping hidden fault at the northern boundary of the Shillong Plateau, parallel to the E–W segment of the Brahmaputra River, was proposed as the Oldham Fault (Bilham & England 2001). The focal mechanism solution of a close earthquake suggested thrust faulting with a significant component of strike-slip motion (Baruah *et al.* 2007). The location of the 110 km long, south-dipping Oldham Fault responsible for the 1897, $M_w = 8.1$ earthquake rupture beneath the Shillong Plateau still remains a matter of controversy (Rajendran *et al.* 2004; Bilham 2006). The presence of major reverse faults on both sides of the Shillong Plateau supports the interpretation in terms of a giant pop-up structure (Bilham & England 2001), with asymmetry indicated by the stronger morphological expression of the Dauki Fault compared with the northern bounding faults. Although the pop-up structure can be explained by N–S compression solely, a dextral component of strike-slip is probably present, according to some focal mechanism solutions suggesting NW–SE compression in and around the Chedrang Valley (Baruah *et al.* 2007).

Baruah *et al.* (1997) studied the seismicity of this region and part of Eastern Himalaya, based on high quality seismic data recorded by the local stations in 1982–1990. The seismic activity is notably high in the depth zone of 10–20 km below the Shillong plateau and the depth zone of 20–30 km below the Mikir Hills. Although the deepest events differ, strike-slip and thrust solutions prevail in the shallow crust down to 40 km depth, with a dominating trend of P-axes suggesting NNW-directed compression. Based on long-baseline geodetic GPS data from 1997–2003 to 2006, Jade *et al.* (2007) showed that within the framework of N–S convergence between Eurasia and India (16 mm yr^{-1}), the present-day deformation is statistically insignificant within the Shillong Plateau and the adjacent Brahmaputra valley and foreland basin to the north.

3 MAIN CHARACTERISTICS OF FOCAL MECHANISM SOLUTIONS IN NE INDIA

The levels of seismic activity are high in Northeast India and adjacent regions (e.g. Thingbaijam *et al.* 2008). In this section, we first present the source and acquisition techniques of our seismological data. We then discuss their main properties in terms of time, location, depth, magnitude and type. Finally, we define nine subzones as a function of geological structure.

3.1 Regional seismic network and waveform inversion

We analysed the earthquakes recorded by the regional seismic networks (RRL-J and NGRI-H), as summarized in the Annual Seismological Bulletin (1982–2006). The precision of hypocenter determination depends not only on the distribution of the recording stations but also on velocity structure between source and station, particularly in area where lateral heterogeneities are extreme (Okada *et al.* 1970). The epicentres were determined using the HYPOCENTER location program of Lienert *et al.* (1986) based on the crustal velocity model of Gupta *et al.* (1984). In our database, most uncertainties involved in the estimates of epicentres and origin times are of the order 0–2 km and 0–0.5 s, respectively. The uncertainties involved in the estimates of focal depths are 0–1 km for 85 per cent and 1–2 km for 15 per cent of the total number of earthquakes located. The depth control is thus reasonably good. To maintain magnitude homogeneity of the data throughout the region, we did not consider in our stress inversions the microearthquake activity analysed by other authors (Kayal & De Reena 1991; Kayal 2001).

In addition to the RRL-J/NGRI-H network data, arrival times reported by the seismic stations maintained by the India Meteorological Department (IMD) at Shillong (SHL), Gauhati University (GAU), Manipur University (MAN) and Mizoram University (AZL) were also used. These stations provided better azimuthal control for determination of hypocentral parameters. Some of these digital seismic stations are equipped with broad-band seismometers, and the waveforms obtained from these stations were also used in this study. GPS time synchronization was maintained with the records. The stations are operated both in continuous and event-trigger mode and recorded at a rate of 100 samples s^{-1}. The recorded seismograms are corrected using an instrument response based on the electrodynamic constant, critical damping, natural frequency of seismometer and bit weight of unit gain of each recording unit for all stations. The events are selected so that these are recorded locally by at least four stations in the considered tectonic 'block', supplemented by at least two more stations in the neighbouring block.

The computation of Green's function is a primary approach for generation of synthetic waveform. Green's functions are calculated using the discrete wavenumber (DW) method (Bouchon 1981 and program AXITRA by Coutant 1989) and convolved with appropriate instrument response and source-time function. The calculated time window length was fixed to 40.96 s; so, the frequency step was $df = 1/40.96 = 0.0244$ Hz. The selection of 4096 complex data

points provided the time increment of the synthetic seismogram of $dt = 0.01$ s. Synthetic amplitude spectra were calculated for the trial values of the scalar moment, strike, dip and rake. The inversion (preferably not below 0.1 Hz) was carried out for a frequency band free of noise (0.2–1.0 Hz and higher signal-to-noise ratio) and completely below corner frequency (ie. 4 Hz). The moment tensor and the Green's tensor were multiplied in complex spectral domain. A correction was applied to compensate the artificial attenuation employed in the DW method, as a regularization and anti-alias operation.

A fine grid search of the strike, dip and rake was performed for the best depth and moment. Then the ray-theoretical first motion polarities were calculated for all strike, dip, rake triplets of the fine grid search and compared with the observed polarities. The misfit function of the amplitude spectrum was considered. A fault plane solution is the final solution when all the observed polarities satisfy the solution with smallest amplitude misfit. Despite differences in misfits of amplitude spectra, the agreements in the time domain were comparable with prime phases, their relative amplitudes and wave group durations. The final validation of the best fitting solutions was accomplished by comparing the observed and synthetic amplitude spectra.

Although most of the focal mechanism solutions used in this study came from the networks described above (Mitra *et al.* 2005, Kayal *et. al.* 2006), the data from the worldwide CGMT system (as developed in Harvard following Dziewonski *et al.* 1981 and Dziewonski & Woodhouse 1983) were taken into additional account.

3.2 Focal mechanism solutions of earthquakes: the data

The total data set, including the data recorded by local networks and the additional CGMT data, contains 285 focal mechanism solutions of earthquakes. The corresponding epicentres are located inside a quadrangle from 20°N to 31°N in latitude and 86°N to 98°N in longitude, representing a total area of nearly 1.5×10^6 km^2. Fig. 3 summarises the distribution of the earthquake data as a function of magnitude (Fig. 3a), time (Fig. 3b) and depth (Fig. 3c).

The recorded magnitudes range from 1.5 to 8.7, with an average magnitude of 5. Less than 4 per cent of the data (11 earthquakes) have magnitudes smaller than 3.5. Low magnitudes are very few (Fig. 3a) because of the relatively low density of the local networks, not to mention the worldwide CGMT records. About 95 per cent of the data (270 earthquakes) have magnitudes from 3.5 to 6.5. The most common magnitude is 5–6 (173 earthquakes, more than half of the data set).

These earthquakes occurred from mid-1950 to mid-2007 (57 yr). The time distributions of Fig. 3 are biased by the increasing sensitivity of the seismological networks. Only 28 events (less than 10 per cent of the data) were recorded during the first half of the considered period. More earthquakes were recorded later because of increased density and technical improvements of the seismological networks in the studied region. Very large destructive earthquakes occurred in 1897 and 1950, with magnitudes of 8.1 and 8.7, respectively. About 20 earthquakes with magnitude 7 or larger have occurred in this region. Few are present in our data list (e.g. the

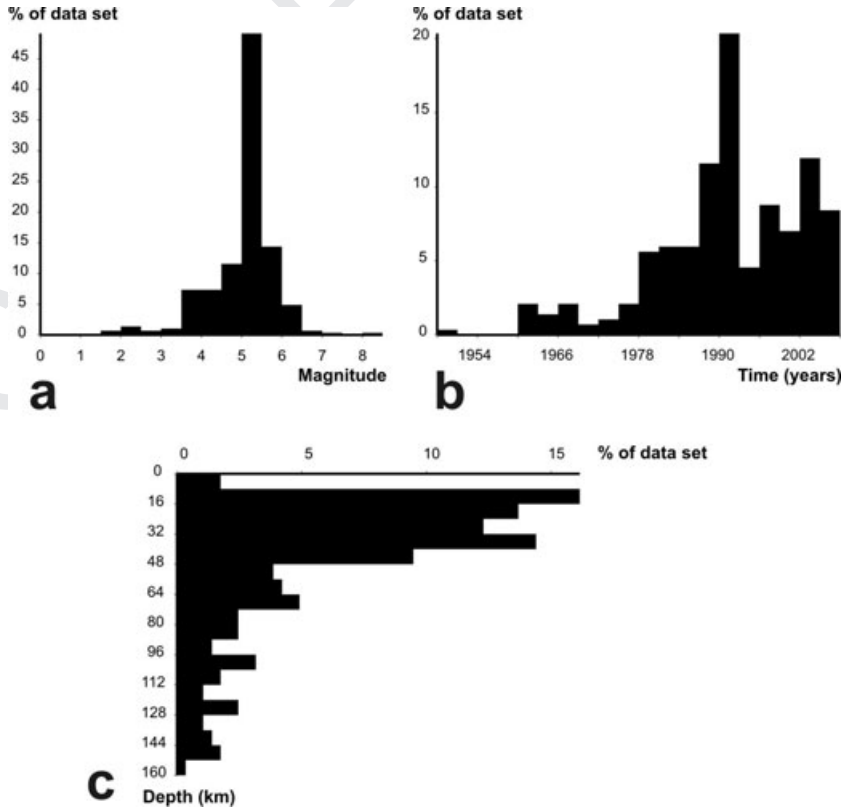

Figure 3. Distribution characteristics of the 285 earthquakes considered in this study. Numbers of earthquakes (as percentages of total data set) as a function of magnitude (a), time (b) and depth (c). As a consequence of the evolution of seismological networks since 1950, histogram (b) does not provide direct expression of changes in natural seismic activity.

Table 1. Distribution of the data set (285 earthquakes) as a function of type (predominantly reverse, strike-slip or normal), as indicated by the steepest plunging axis (P, B or T, respectively).

Subset	Proportion of total set (per cent)	Average magnitude	Average depth
Total	100	5.0	46
Reverse	37	5.1	54
Strike-slip	41	4.9	42
Normal	22	5.0	40
Compression	64	5.0	50
Extension	36	5.0	40

Note: Compression and extension refer to the same data set but are derived in a different way (steepest plunging axes P and T respectively, as explained in text). For each subset, average magnitude and depth (in km) are indicated.

large 1950 earthquake) but most are absent (e.g. the 1897 large earthquake) because good focal mechanisms solutions were not available. 91 earthquakes (32 per cent of the data) were recorded between mid-1990 and mid-1993, indicating higher tectonic activity.

Most events (66 per cent of the data, i.e. 188 earthquakes) occurred at crustal depths between 8 and 48 km (Fig. 3c). For 90 per cent of the data, depths are shallower than 100 km. The average depth is 46 km. Earthquakes deeper than 90 km occur only beneath the Indo–Burma Ranges. Adopting a thickness of 50 km for the domain where data are abundant, a crustal volume of about 75×10^6 km^3 is illuminated by more than two-thirds of the 285 focal mechanisms analysed herein.

We distinguished predominantly reverse, strike-slip and normal types (Table 1). The simplest way to separate these three types involves consideration of the steepest plunging axis (P for normal, T for reverse and B for strike-slip). The B-axis of a double couple mechanism is the intersection of the nodal planes, whereas the P- and T-axes, respectively, bisect the pressure and tension right dihedra formed by these planes. The strike-slip and reverse-type mechanisms represent 41 and 37 per cent, respectively, whereas the normal-type subset is minor (22 per cent). We also distinguished 'compressive' and 'extensional' types. A P-axis steeper than the T-axis indicates predominating extension, whereas a T-axis steeper than the P-axis indicates predominating compression. This geometrical distinction only affects the predominantly strike-slip subset, split into compressive and extensional components. Thus, only 36 per cent of the total set is extensional in type, whereas 64 per cent of the earthquakes are compressive. The difference in average magnitude between all these subsets is not significant, but the average depth is larger by about 10 km for reverse-type earthquakes compared with strike-slip and normal types (Table 1).

3.3 Definition of subzones

The map of Fig. 4 shows the distribution of focal mechanism solutions as a 'beachball', with compressive quadrants left white and extensional quadrants black in equal-area stereoplots. Fig. 4 also shows the boundaries of the nine subzones analysed in the following sections. These subzones have been determined as a function of both the seismic activity distribution and the major structural units of the region (Fig. 2). To the north, the three subzones of Bhutan Himalaya (1), Arunachal Himalaya (2) and Mishmi Thrust (3) belong to the Eastern Himalaya. To the southeast, the three subzones of S and E Indo–Burma regions (7 and 8, respectively) and Sagaing Fault Region (9) belong to the Indo–Burma Ranges. Between these two main mountainous domains, the intraplate domain of Northeast India has been subdivided in three subzones: Tripura Belt (4); Shillong Plateau (5) and Assam Valley (6), from southwest to northeast.

As a comparison between Figs 2 and 4 shows, the boundaries between these subzones differ in nature. Primary boundaries separate the major structural domains (Table 2: A, Himalayas; B, Northeast India and C, Indo–Burma Ranges). Secondary boundaries separate segments with different orientations within a belt (lines 1–2 for Himalayas and 7–8 for Indo–Burma Ranges) or different structural domains (line 2–3 between Himalaya and Mishmi Block), inner and outer zones in the Burmese orogen (lines 7–9 and 8–9) and different domains of the Indian Plate (lines 4–5 between the Bengal Basin–Tripura Belt and the Shillong Plateau, 5–6 coinciding with the Kopili lineament across the Assam Valley).

The dips of major boundaries have been taken into account where appropriate, especially near the major front thrust zones of the Himalaya and Indo–Burma Ranges. The main properties of these subzones are summarized in Table 2 in terms of regional names, numbers, depths and magnitudes of earthquakes, as well as types of nodal planes.

4 COMPATIBILITY BETWEEN EARTHQUAKE MECHANISMS IN NE INDIA: PRELIMINARY ANALYSES

Prior to accurate stress determinations inside the subzones defined above, it is appropriate to determine whether or not a limited number of stress states may account for the focal mechanism solutions of earthquakes observed in the whole studied area.

4.1 Insights from distributions of B, P and T axes

A simple—albeit mechanically questionable—account of the distribution of earthquake mechanisms in the area of Fig. 4 is provided through geometrical consideration of the attitudes of the individual axes of double couple focal mechanism solutions of earthquakes. This analysis has been done in the descending Indian plate and the overriding Burma plate (Khan 2005). The P- and T-axes have no rigorous mechanical significance; considering that they, respectively, reveal the axes of maximum and minimum stress would require unrealistic assumptions of perfectly homogeneous, isotropic and elastic crust. However, considering P- and T-axes paves the way for a geometrical and mechanical classification of solutions.

In Fig. 5, rose diagrams summarise the distributions of trends and plunges of the B-axes (describing the intersection of nodal planes) and the P- and T-axes (that, respectively, bisect the pressure and tension right dihedra formed by the nodal planes). B-axes

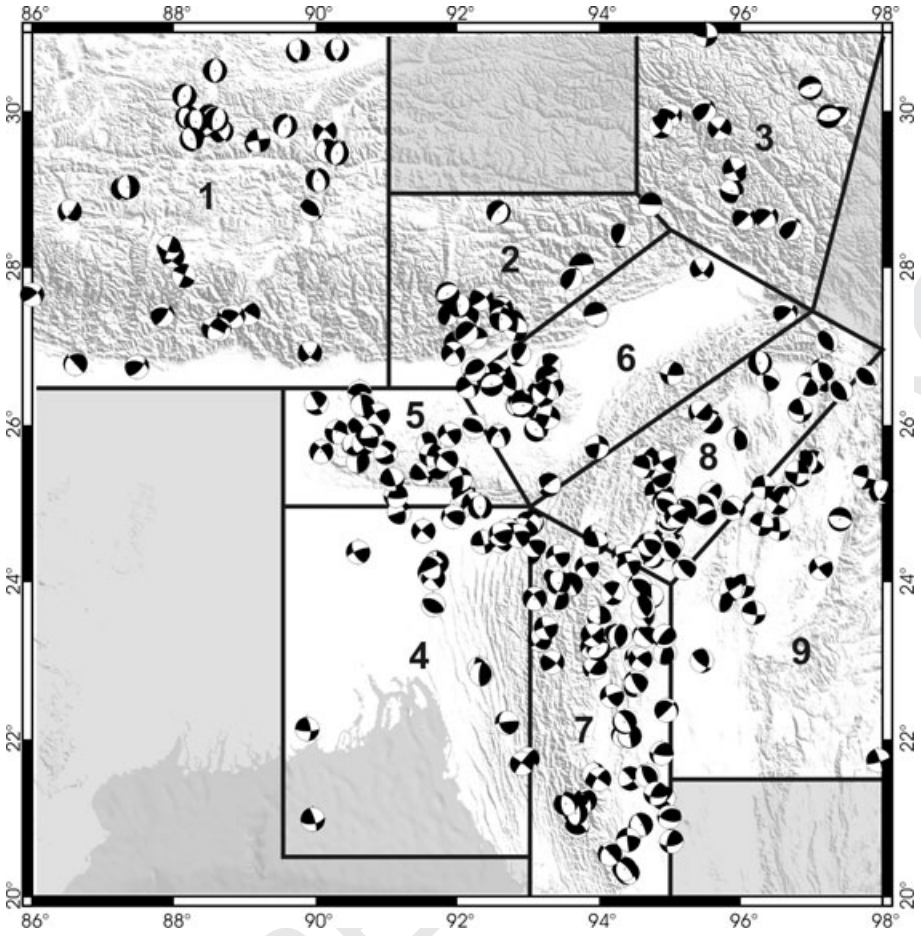

Figure 4. Map distribution of epicentres of the 285 earthquakes considered in this study. All earthquakes shown with the conventional illustration as 'beachball' (Schmidt's, equal area stereoplot, lower hemisphere, with extensional quadrants black and compressive quadrants left white). Subzones analysed in this paper numbered 1–9, with boundaries as thick lines. Bhutan Himalaya (subzone 1), Arunachal Himalaya (subzone 2) and Mishmi Thrust (subzone 3) belong to Eastern Himalaya. Tripura Belt (subzone 4), Shillong Plateau (subzone 4) and Assam Valley (subzone 6) belong to Northeast India. Southern Indo–Burma region (subzone 7), eastern Indo–Burma region 8 (subzone 8) and Sagaing Fault region (subzone 3) belong to Indo–Burma Ranges (see also Table 2).

Table 2. Distribution within subsets according to earthquake location (see map of Fig. 4).

		Number		Depth			Magnitude			Type		
		S-Z	Z	min	max	ave	min	max	ave	N	R	SS
	Total	285		2	153	46	1.5	8.7	5.0	124	214	232
A	Bhutan Himalaya: 1	40	79	9	86	33	3.5	6.5	5.3	40	14	26
	Arunachal Himalaya: 2	23		4	83	26	3.5	5.9	4.8	6	28	12
	Mishmi Thrust: 3	16		10	4	26	4.5	8.7	5.4	8	12	12
B	Tripura Belt: 4	29	79	2	103	35	3.8	6.1	5.2	2	22	34
	Shillong Plateau: 5	25		5	62	23	1.5	5.3	3.8	2	20	28
	Assam Valley: 6	25		9	56	32	3.4	5.4	4.5	14	12	24
C	S Indo–Burma Region: 7	61	127	10	143	67	3.6	6.2	5.0	38	44	40
	E Indo–Burma Region: 8	45		15	153	77	3.5	7.2	5.3	10	49	31
	Sagaing Fault Region: 9	21		7	120	37	4.9	6.9	5.4	4	12	26

Note: Main zones: A, Eastern Himalaya; B, Northeast India; C, Indo–Burma Ranges.
Subzones with names indicated, numbered 1–9. Number: number of focal mechanism solutions (S-Z, subzones; Z, main zones).
Depths (in km) and magnitudes indicated as smallest (min), largest (max) and average (ave) values.
Type of focal mechanism solution indicated as normal (N), reverse (R) or strike-slip (SS), with corresponding numbers of nodal planes. As each solution includes two nodal planes, the last three columns together contain twice the number of events.

show scattered trends and a variety of plunges, from horizontal to vertical (Fig. 5a). This large dispersion results from the association of strike-slip, reverse and normal focal mechanism solutions. Because strike-slip focal mechanism solutions are abundant, many plunges of B-axes are steep, which results in increased dispersion of their trends. In contrast, the P-axes reveal typical concentration around shallow, often nearly horizontal, plunges and N–S trends (Fig. 5b). Such a distribution suggests that many E–W trending dip-

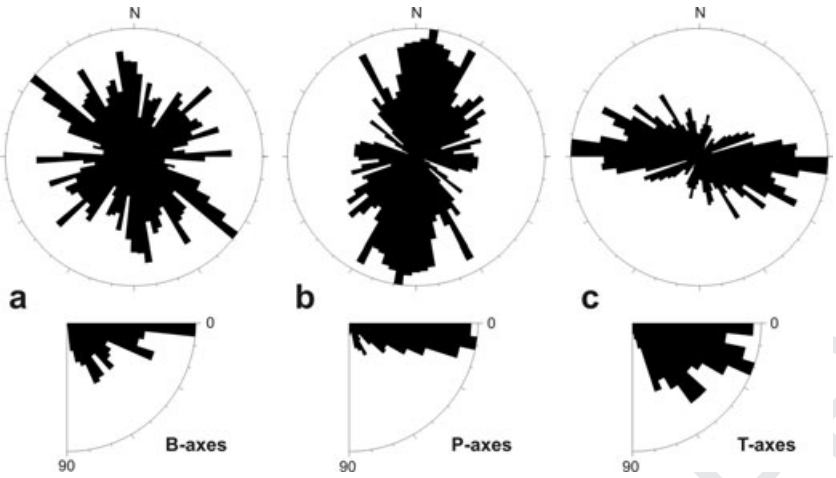

Figure 5. Rose diagrams showing the angular distribution of trends (upper row, N indicates north) and plunges (lower rows, values in degrees) of the individual B-axes (a), P-axes (b) and T-axes (c), for the 285 earthquakes considered in this study.

slip reverse faults, NW–SE (right-lateral) and NE–SW (left-lateral) strike-slip faults may be present, which is consistent with structural observations in the area (Fig. 2). Small but significant subsets of NNW–SSE, NNE–SSW and even E–W trends of P-axes are also present. The rose diagram of trends reveals high concentration of T-axes around E–W (Fig. 5c), which considering the dominating N–S trend of P-axes suggests that strike-slip faults with NW–SE and NE–SW strikes (right-lateral and left-lateral in sense, respectively) play a large role. However, many steeply plunging T-axes are present, consistent with reverse faulting.

4.2 P and T dihedra analysis of the entire data set

A more rigorous approach of stress indicated by the focal mechanism solutions of Fig. 4 is possible, using the right dihedra (or P and T dihedra) method. This method consists of mapping the probability distribution of pressure and tension on the sphere (Angelier & Mechler 1977). It is applicable to double couple focal mechanism solutions of earthquakes and does not require any choice between the nodal planes. The principle is simple: if all shears independently occur as function of a single stress state, the principal stress axis σ_1 (maximum compressive stress) belongs to the solid angle common to all pressure dihedra, whereas the principal stress axis σ_3 (minimum stress) is in the solid angle common to all tension dihedra. As natural dispersion, stress heterogeneity and fault interactions occur, not to mention measurement uncertainties, the method is used in terms of proportions, from –1 (100 per cent pressure) to 1 (100 per cent tension). This analysis allows easy 3-D visual evaluation of consistency between double couple mechanisms (Fig. 6).

Fig. 6 shows the application of this method to the 285 earthquake mechanisms. For each direction in space, the proportion of pressure and tension is graphically illustrated by a level of grey, ranging from bright white (100 per cent pressure) to black (100 per cent tension). With the entire data set, a low-contrast diagram is obtained (Fig. 6a), which indicates a low level of mechanical compatibility (51 per cent for pressure and 40 per cent for tension, Table 3). Thus, a single state of stress cannot account for the whole set of focal mechanism solutions. The trend of the preferred axis for pressure (Fig. 6a) is close to N–S, similar to the peak trend of P-axes (Fig. 5).

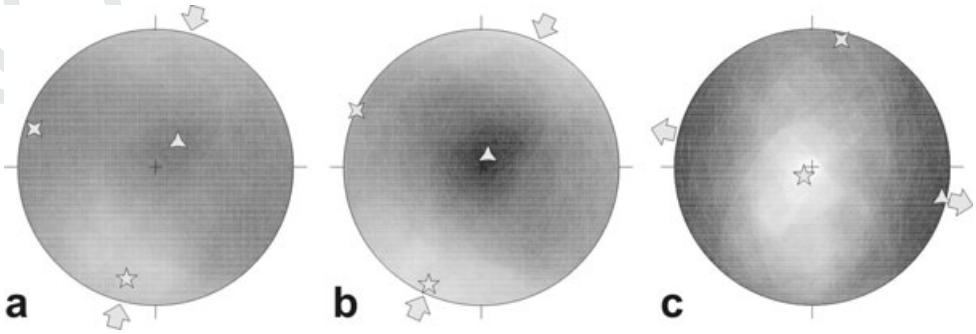

Figure 6. Stereoplots showing the density distribution of pressure and tension on the sphere for the 285 earthquakes considered in this study, according to the method described by Angelier & Mechler (1977). Schmidt's, equalarea projection, lower hemisphere. Bright white indicates 100 per cent pressure, gradually darker levels of grey indicate increasing proportion of tension relative to pressure, and black indicates 100 per cent tension. Preferred axes of maximum pressure (5-branch star) and maximum tension (3-branch star), as well as intermediate, perpendicular axis (4-branch star), are added. These axes reflect statistically determined extrema, not optimum principal stress axes σ_1, σ_3 and σ_2 (maximum compressive stress, minimum stress and intermediate principal stress, respectively). Large arrows show the inferred trends of compression (convergent pairs of arrows) and extension (divergent ones). (a) whole set of data, with 285 earthquake focal mechanism solutions. (b) compressive subset, including 182 mechanisms. (c) extensional subset, including 103 mechanisms. The definition of compressive and extensional subsets is given earlier in text.

Table 3. Results of the right dihedra method for the total data set (285 earthquakes) and the compressive and extensional subsets (as defined in text).

Subset	Fig.	Number of earthquakes	Maximum pressure (per cent)	Maximum tension (per cent)	Preferred axis, P	Preferred axis, T	Estimated ratio Φ
Total	6a	285	51	40	195–18	42–70	0.6
Compression	6b	182	67	100	204–08	29–82	0.6
Extension	6c	103	100	77	224–83	103–4	0.4

Note: Maximum P and T ratios refer to the largest proportion of pressure and tension dihedral, respectively. The corresponding axes are the barycentres of the maximum compatibility domains on the sphere and should not be regarded as optimum stress axes (orientation given as trend and plunge in degrees). The estimated ratio Φ results from raw evaluation of the 3-D distribution pattern of P and T dihedra. Φ is the ratio between principal stress differences $\Phi = (\sigma_2 - \sigma_3)/(\sigma_1 - \sigma_3)$. The value of Φ ranges from 0 to 1. Detailed explanation of the method in Angelier and Mechler (1977).

4.3 P and T dihedra analysis: definition of subsets

The same analysis was applied to the compression and extension subsets defined in Table 1. In the compressive subset (Fig. 6b), the maximum compatibility, 100 per cent, is obtained for tension (near the centre of the stereoplot), whereas for pressure there is no compatibility higher than 67 per cent. In the extensional subset (Fig. 6c), pressure compatibility reaches 100 per cent (also near the vertical), but the best tension compatibility is only 77 per cent. Thus, despite apparent consistency, the stress regimes cannot be regarded as homogeneous, even in the first approximation, a conclusion that could be expected considering the size and complexity of the studied area (Figs 2 and 4).

However, within the range of uncertainties, all diagrams of Fig. 6 suggest the same trend of maximum horizontal compressive stress. The difference between the right dihedra distributions of Figs 6(b) and (c) can be regarded as a circular permutation between preferred principal axes; within non-significant angular variations of few degrees, axes σ_1, σ_2 and σ_3 in Fig. 6(b), respectively, become σ_2, σ_3 and σ_1 in Fig. 6(b). A more detailed approach requires consideration of the spatial distribution of earthquakes (Fig. 7 and Table 4).

In the Eastern Himalaya domain, the N–S compression associated with E–W extension prevails. This compression is nearly perpendicular to the E–W trending belt front (Bhutan Himalaya, subzone 1). The Arunachal Himalaya (subzone 2), where the belt front trends ENE–WSW, shows counter-clockwise deviation of compression, approximately perpendicular to the major thrusts. The Indo–Burma Ranges show quite different trends of compression: NE–SW on average, which remain constant despite the major clockwise change that affects the structural grain trend to the north (Fig. 2). The Northeast India intraplate domain shows intermediate orientations, with a NNE–SSW trend of compression to the southwest (Tripura Belt, subzone 4) and a gradual change to NNW–SSE toward the northeast (Assam Valley, subzone 6). The compression beneath the Shillong Plateau (subzone 5) resembles in trend that of the Bhutan Himalaya.

The right dihedra analyses of subsets selected according to faulting type (Fig. 6 and Table 3) and location (Fig. 7 and Table 4) differ. In the first case, at least one percentage of 100 per cent is reached despite large subset size and data dispersion (Table 3), which suggests overall mechanical consistency. For spatially defined subsets, no percentage is higher than 91 per cent and values as low as 60 per cent are common (Table 4), despite the smaller size of these subsets. Thus, not only is the homogeneity of the whole data set severely affected by regional contrasts, but also each zone contains incompatible mechanisms. For this reason, the determination of stress in the studied area requires consideration of both the differences in mechanisms according to faulting modes and the regional changes that depend on the distribution of major seismotectonic units.

Despite encouraging results (Fig. 7), the right dihedra method provides quantification of mechanical consistency levels, not the determination of stress regimes done in the next section.

5 STRESS INVERSION OF EARTHQUAKE MECHANISMS: AVERAGE SEISMOTECTONIC REGIMES

The average seismotectonic regimes that prevail in the same subzones as in Figs 3 and 7 are accurately determined using the inversion of double couple focal mechanism solutions of earthquakes to determine best-fitting stress tensors.

5.1 The inverse method

One cannot reasonably expect stress to be unique within a time span of 57 yr and volumes of millions of cubic kilometres, as it would be at a single point in space and time. The stress in the lithosphere is subject to large changes that depend on a variety of phenomena (in space: irregular distribution of boundary and volume forces, mechanical discontinuities and anisotropies, variable thermal status, etc.; in time: elastic rebound, creep and variable mechanical coupling along faults, fluid migration, etc.). Even within structurally defined subsets (Figs 4 and 7), stress heterogeneity was expected and effectively observed in such large volumes and time span. Inversion with separation into mechanically homogeneous subsets is discussed in Section 5.

Our stress determinations are all based on a single analytical inversion described by Angelier (2002) in a methodological paper that also contained general information about the principles and related references. This inverse method, as all other stress inversions, derives from both the general principle of stress-slip relationships first presented by Wallace (1951) and re-formulated by Bott (1959) and the first formulation and resolution of the inverse problem by Carey & Brunier (1974). The inversion reveals the stress state that best accounts for a set of double couple focal mechanism solutions of earthquakes. For a mechanically homogeneous subset, one obtains optimum stress axes σ_1, σ_2 and σ_3 and the ratio of principal stress differences, $\Phi = (\sigma_2 - \sigma_3)/(\sigma_1 - \sigma_3)$, as well as related average and individual uncertainties. The number of unknowns of the reduced stress tensor is four for many focal mechanism solutions, so that the inverse problem is overdetermined (e.g. Angelier 1984, 1989). Therefore, not only does the inversion reveal the stress state, it also allows accurate evaluation of consistency levels.

The inverse method adopted resembles the direct inversion method described for fault slips (Angelier 1990), but the physical criteria and the derivations differ. It does not require any choice between the nodal planes (Angelier 2002). We used the Tector 2000 softwares (technical information available at http://jacques.angelier.googlepages.com/). Analytical tools reduce

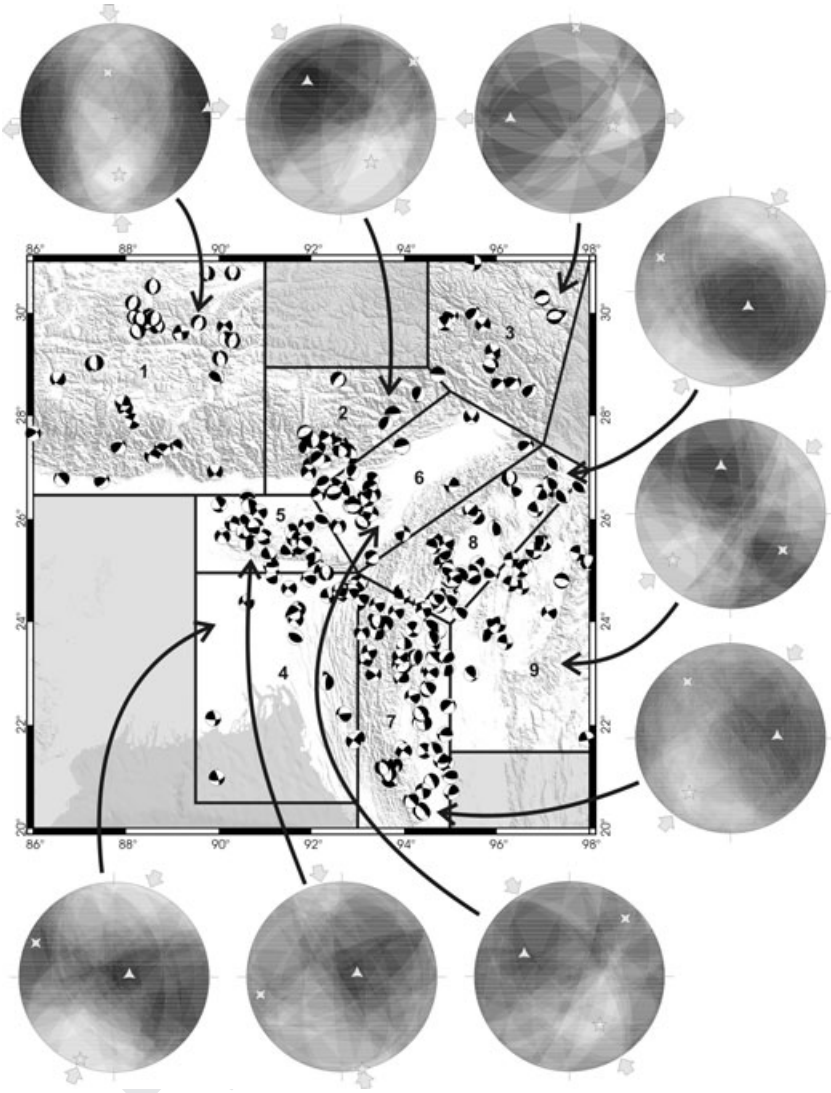

Figure 7. Stereoplots showing the density distribution of pressure and tension on the sphere for all spatially defined subsets of Fig. 3 and Table 2. Same caption as for Fig. 6.

Table 4. Results of the right dihedra method for spatially defined subsets (as indicated in Fig. 4 and Table 2). Same caption as for Table 3.

Subset	Number of earthquakes	Maximum pressure (per cent)	Maximum tension (per cent)	Preferred axis, P	Preferred axis, T	Estimated ratio Φ
1	40	85	85	177–40	84–3	0.4
2	23	91	91	145–44	319–46	0.4
3	16	75	69	100–52	270–37	0.4
4	29	79	86	202–7	80–77	0.5
5	25	60	76	168–0	77–77	0.5
6	25	68	60	148–40	297–46	0.6
7	61	70	64	217–29	87–49	0.3
8	45	78	78	28–5	131–70	0.6
9	21	71	71	231–23	349–47	0.4

numerical aspects to a minimum so that runtime is short and the inversion can be encapsulated in a variety of processes to refine the data or separate stress states. The inversion involves maximization of the slip shear stress component (SSSC), the component of stress acting in the slip direction of a fault. A double couple focal mechanism solution of earthquake includes two possible, mutually exclusive, fault slips. If the focal mechanism and the stress tensor are perfectly consistent, the SSSC value is unique regardless of the nodal plane acting as the fault. This mechanical property explains why the SSSC-based inversion avoids the undesirable effects of the intrinsic ambiguity between nodal planes in double couple focal mechanism solutions. This choice can be done after the inversion

but is not discussed hereafter to preclude artificial improvement in fit levels. To perform inversion, ω, the SSSC divided by the maximum shear stress τ_{max}, is made maximum. The SSSC is the product of the shear stress, τ, by the cosine of the shear-slip angle, α. Maximizing ω aims at obtaining shear stress as large as possible (ideally, $\tau = \tau_{max}$) and parallel to slip with the same sense (ideally, $\alpha = 0$). The inversion thus provides the smallest slip-shear angles and the largest possible shear stresses that can simultaneously exist for all the data. The value of ω ranges from –100 (total misfit, $\tau = \tau_{max}$ in the direction opposite to slip) to +100 per cent (perfect fit, $\tau = \tau_{max}$ in the direction of slip). A zero value indicates null shear stress or shear stress τ perpendicular to slip, as the limit between consistent and inconsistent senses of motion. The minimum angle condition for α aims at obtaining directions as close as possible for theoretical and actual slips. For sets of nodal planes with a variety of orientations and significant number of data, the most important constraint results from the minimum angle condition.

In the inversion process, the normalized sum of SSSC values is maximized as a function of three unknowns that control the orientation of the stress tensor and the ratio Φ of principal stress differences. To evaluate the significance of stress determinations, we adopted a refining process with repeated inversions and increasing individual fit demand, as already applied in Taiwan (Angelier 2002) and Iceland (Angelier *et al.* 2004, 2008), with detailed explanation.

The real data dispersion is much larger than the average technical angular uncertainty of 5°–20° in the determination of individual focal mechanism solutions that we used. This uncertainty depends on several factors, including earthquake magnitudes as well as number and distribution of recording seismological stations. Additional uncertainty results from natural dispersion and stress perturbations in a large volume. All results displayed hereafter correspond to a single threshold value, $\omega_{acc} = 0.4$, meaning that individual data with ω smaller than 40 per cent are considered unacceptable. This value is consistent with the average accuracy of focal mechanism solutions. It would have been good to consider variations of ω_{acc} as a function of the angular accuracy of each focal mechanism solution, but this information was absent for many earthquakes.

Examining the number of rejected data for a realistic largest acceptable misfit is crucial while evaluating the quality and reliability of the inversion. A severe fit demand resulting in large data rejection would artificially provide good average misfits and small standard deviations. Thus, not only does a good result imply low average misfit indicated by high ω value, it also requires a low rejection rate. A major criterion is the stability of the results throughout the refining process: for all inversions below, the variation in orientations of stress axes and ratio Φ, monitored while ω_{acc} increased, was found minor, highlighting stability in the inversion.

5.2 Application to nine subzones of NE India

The results of stress inversions obtained for the nine regional subsets defined in Fig. 4 (see also Table 2) are listed in Table 5 and illustrated in Fig. 8. These results are more accurate than, but generally consistent with, the probability distributions revealed by the right dihedra analysis (Fig. 7 and Table 4).

Confidences ellipses and azimuthal standard deviations are given in all stereoplots. For instance, in Fig. 8, the confidence ellipses around σ_1 and the standard deviation around the related direction of compression are large for subzone 2 and small for subzone 4, which reveals high contrasts in dispersion levels. Significant differences in stress orientations occur (compare Figs 7 and 8); this is the case in subzones of Mishmi Thrust (3), Shillong Plateau (5) and Assam Valley (6), revealing instability as quite different stress states are mixed in these subzones located between the Himalayas and the Indo–Burma Ranges.

The focal mechanism solutions of the Eastern Himalaya domain reveal compression that trends NNW–SSE to N–S on average in subzones of Arunachal Himalaya (2) and Mishmi Thrust (3). In Bhutan Himalaya (1), this N–S compression is typically associated with E–W extension. In contrast, the Indo–Burma Ranges reveal a NE–SW average trend of compression in the three subzones. Between these two domains, the Northeast India domain shows a dominating compression that approximately trends N–S in all subzones, regardless of their position between the major mountain

Table 5. Results of the inversions of focal mechanism solutions for the nine regional subsets.

N_z	Acc	Rej	σ_1		σ_2		σ_3		Φ	ω_m	$\tau*$	α
			d	p	d	p	d	p		(per cent)	(per cent)	(deg)
1	28	12	298	87	178	2	88	3	0.73	79±14	85±12	17±12
2	19	4	159	32	65	7	324	57	0.47	69±18	78±16	24±17
3	8	8	169	9	71	43	268	46	0.47	76±17	84±13	21±15
4	20	9	196	2	296	78	105	12	0.28	77±14	83±13	17±13
5	13	12	189	21	295	36	75	47	0.48	66±15	75±16	23±16
6	12	13	177	35	68	26	310	45	0.61	67±17	75±16	24±16
7	40	21	207	33	324	36	88	38	0.77	67±14	76±14	24±16
8	33	12	30	4	297	30	126	59	0.47	73±16	81±16	21±14
9	14	7	236	9	126	65	330	23	0.32	76±17	80±15	16±14

Note: Detailed explanation of the inversion method in Angelier 2002. After application of the refining process, the stage with a 40 per cent threshold value of ω is displayed for all subsets.

Nz, reference number of subzone, as defined in Fig. 4 and Table 2; Acc, number of accepted mechanisms; Rej, number of rejected mechanisms ($\omega < 40$ per cent).

Stress axes with orientation given as trend (d) and plunge (p), in degrees. Φ, ratio of principal stress differences as defined by Angelier (1975, 1989), $\Phi = (\sigma_2 - \sigma_3)/(\sigma_1 - \sigma_3)$.

Main *a posteriori* estimator ω_m from –100 (total misfit) to 100 per cent (perfect fit), with average value and standard deviation.

Auxiliary estimators τ^* and α, so that $\omega = \tau^* \cos\alpha$.

τ^*, average shear stress as percentage of maximum shear stress from 0 to 100 per cent; α, average angle between observed slip and calculated shear stress. These average estimators are calculated for all accepted nodal planes, without any choice between nodal planes.

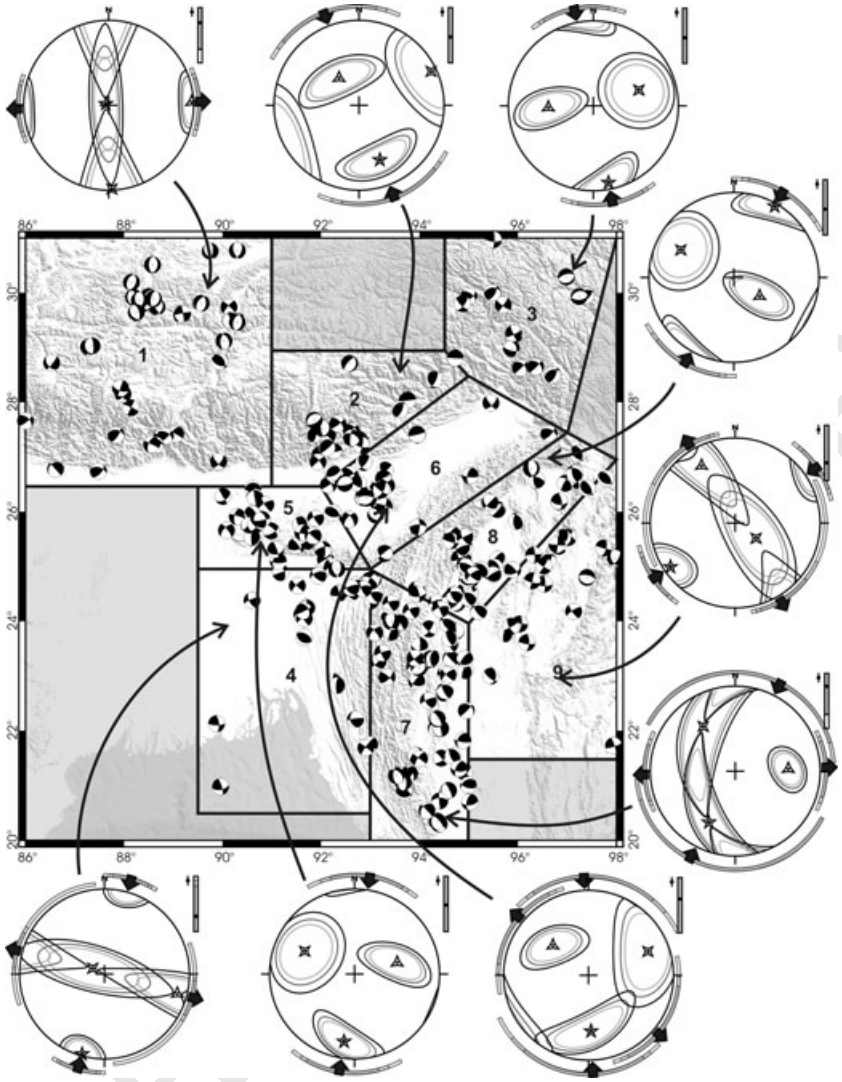

Figure 8. Result of inversions to obtain the average stress tensor according to Angelier's method (2002) for the spatially defined subsets of Fig. 4 and Table 2. Beachball map as in Fig. 4. Stereoplots: equal-area projection, lower hemisphere. All inversions shown for a 40 per cent threshold value of ω (see text), with stress axes σ_1, σ_2 and σ_3 as 5, 4 and 3-branch stars, respectively. Scale bar of Φ value added in upper-right-hand corner for each stereoplot ($\Phi = 0$ at base, $\Phi = 1$ at top). Pairs of black arrows indicating trends of compression (convergent) and extension (divergent). Confidence ellipses (60, 75 and 90 per cent) shown for each stress axis, standard deviations indicated by three levels of grey in thick arcs of circle around the trends of extension and compression, and also for the Φ value.

belts (Shillong Plateau and Assam Valley, respectively, 5 and 6) or farther west in the Indian plate (Tripura Belt, 4).

5.3 Limitations: data heterogeneity

Despite their general consistency, the above stress determinations are not satisfactory for three reasons. First, the rejection rate is high, up to more than 50 per cent in the southern Indo–Burma region (subzone 7; compare the second and third columns in Table 5). Second, despite this high rejection rate, the average fit levels for the remaining acceptable data are poor. Third, most stress tensors obtained show oblique patterns with inclined axes (Fig. 8), which often occur at depth in descending slabs but is uncommon in the horizontal, upper lithosphere. All this indicates high levels of heterogeneity in seismotectonic stress, in agreement with the conclusions of Section 3.

6 STRESS INVERSIONS OF EARTHQUAKE MECHANISMS: HOMOGENEOUS SEISMOTECTONIC REGIMES

Because of the unacceptable levels of heterogeneity in the determination of average stress states (Table 5 and Fig. 8), we carried out a systematic separation using a dynamic clustering method coupled with stress inversions.

6.1 Coupled inversion and subset separation

The inversion is the same as in Section 4, but it is included in a dynamic separation process. This process, described by Angelier (1984) for another type of stress inversion, allows distinction of homogenous data subsets within heterogeneous populations. The results are listed in Table 6 and illustrated in Figs 9, 10 and 11

Table 6. Results of stress inversions coupled with stress separation of focal mechanism solutions for the nine regional subsets.

Z	Sbs	ω_{min}	N	U	σ_1		σ_2		σ_3		$\Phi\omega_m$		$\tau^*\alpha$	
		(%)			d	p	d	p	d	p		(per cent)	(per cent)	(degrees)
1	a	45	13	5	168	14	19	73	260	8	0.20	81 ± 16	89 ± 6	19 ± 18
	b	50	22		350	85	182	5	92	1	0.59	83 ± 12	87 ± 12	14 ± 9
2	45	18	5	157	32	61	9	317	57	0.47	70 ± 16	79 ± 15	23 ± 15	
3	a	40	8	3	169	9	71	43	268	46	0.47	76 ± 17	84 ± 13	21 ± 15
	b	40	5		32	71	271	10	178	15	0.44	68 ± 26	75 ± 24	21 ± 15
4	a	40	11	6	187	9	305	71	94	16	0.36	84 ± 11	88 ± 9	12 ± 13
	b	40	12		34	1	303	27	126	63	0.06	82 ± 11	91 ± 6	22 ± 14
5	a	45	12	3	192	11	88	50	291	38	0.15	74 ± 15	86 ± 11	25 ± 17
	b	45	10		280	29	179	20	59	54	0.13	68 ± 17	82 ± 13	30 ± 17
6	a	60	9	8	176	13	55	65	271	20	0.48	77 ± 10	82 ± 11	15 ± 11
	b	50	8		99	25	212	39	346	40	0.76	81 ± 11	86 ± 11	16 ± 11
7	a	40	21	7	16	1	286	50	107	40	0.40	73 ± 18	81 ± 15	21 ± 15
	b	60	13		269	19	179	1	85	71	0.18	82 ± 9	89 ± 8	18 ± 12
	c	45	20		212	62	338	17	75	22	0.47	76 ± 17	81 ± 15	18 ± 13
8	a	50	20	3	229	4	321	22	130	68	0.37	84 ± 13	88 ± 11	14 ± 12
	b	40	15		353	18	254	26	114	57	0.42	76 ± 19	84 ± 17	20 ± 16
	c	50	7		49	62	200	25	295	12	0.74	77 ± 11	86 ± 10	22 ± 15
9	a	60	7	4	263	11	155	59	359	29	0.26	82 ± 11	88 ± 8	18 ± 13
	b	40	10		222	8	106	72	314	16	0.33	79 ± 18	83 ± 16	13 ± 12

Note: Inversion method from Angelier (2002), included in dynamic clustering to separate stress states (Angelier 1984). In the separation process, subsets below the 40 per cent threshold value ω_{acc} cannot be built.
Z, reference number of subzone, as defined in Fig. 4 and Table 2; Sbs, reference index of stress regime, as for the stereoplots of Figs 9–11.
Final minimum value obtained for each subset, ω_{min}.
N, number of accepted mechanisms; U, number of unclassified mechanisms.
Other columns refer to the same parameters as in Table 3 (stress axes with orientation given as trend and plunge in degrees, ratio Φ of principal stress differences, main *a posteriori* estimator ω_m and auxiliary estimators τ^* and α).

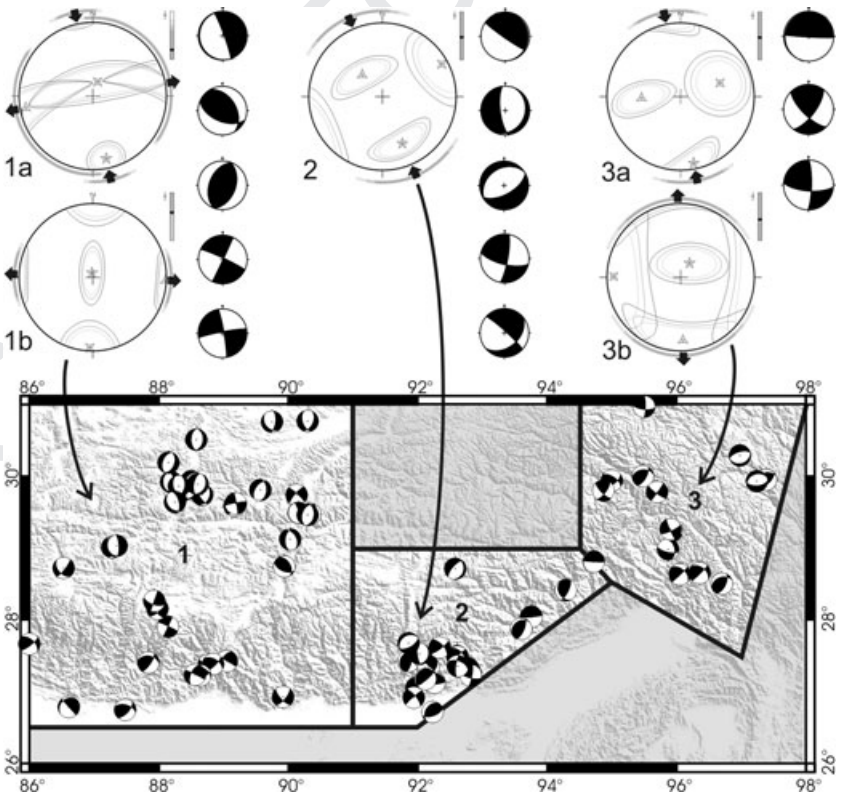

Figure 9. Results of stress inversions coupled with stress separation of focal mechanism solutions for the Eastern Himalaya subsets (1 Bhutan Himalaya, 2 Arunachal Himalaya and 3 Mishmi Thrust, as defined in Fig. 4 and Table 2). For stereoplots, same caption as for Fig. 8. Numerical characteristics of all determinations listed in Table 6, with identical reference numbers of subzones and indexes of stress regimes.

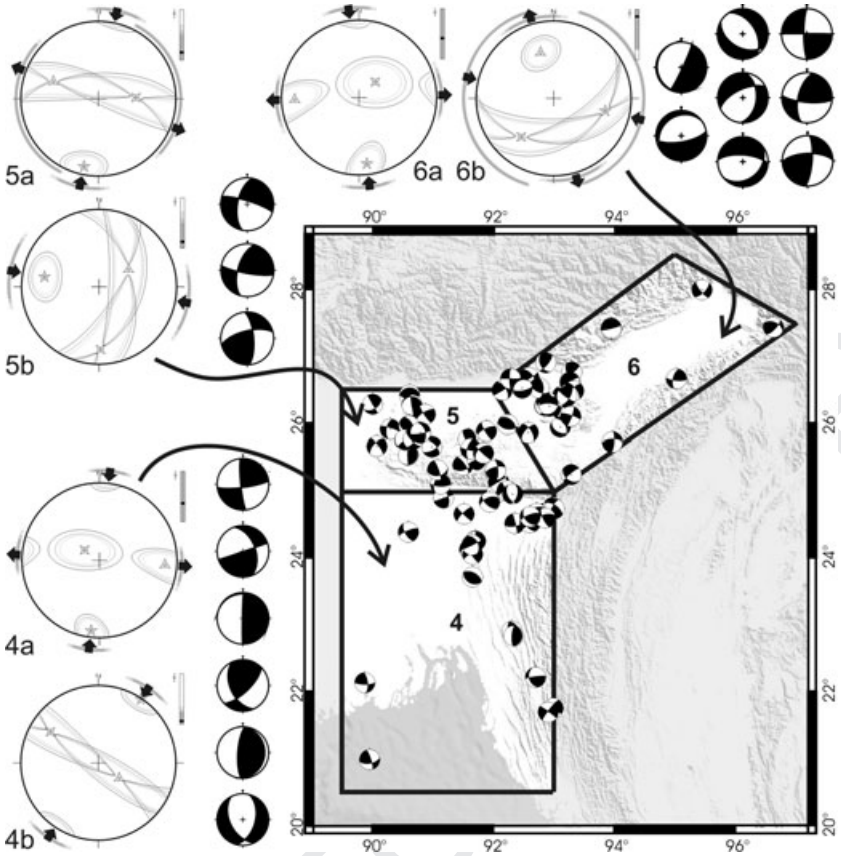

Figure 10. Results of stress inversions coupled with stress separation of focal mechanism solutions for the Northeast India subsets (4 Tripura Belt, 5 Shillong Plateau and 6 Assam Valley; see Fig. 4 and Table 2). Other explanations as for Fig. 9. See also Table 6.

for the Eastern Himalaya, Northeast India and Indo–Burma Ranges domains, respectively.

Before discussing the regional aspects, it is worth pointing out that the stress cannot be reliably determined with very small numbers of earthquakes, so that after the separation process, some focal mechanism solutions remain unclassified (U-column in Table 6) and cannot constitute a stress-consistent subset large enough to allow reliable stress determination. One should also note that all determinations are not equally significant, with poor quality for the smallest subsets and good quality for the largest ones (e.g. 3b and 1b, respectively, in Table 6). Whether the remaining, unclassified mechanisms, reflect wrong determinations or significant but 'isolated' earthquakes, cannot be decided based on the present stress analysis but requires seismological re-examination of the data. In Figs 9–11, these unclassified mechanisms are shown as separate beachballs on the right of the stereoplots that illustrate the identified stress states.

6.2 Eastern Himalayas

Regarding the regional subsets of Eastern Himalayas (Fig. 9), the level of stress heterogeneity remains moderate. Only one or two stress states were returned by the separation process. The direction of compression does not significantly vary, N165°E ($\pm$ 16°) on average.

In the subzone of Bhutan Himalaya (1), the low Φ ratio favours permutation between σ_2 and σ_3, consistent with the shape of confidence ellipses forming a girdle perpendicular to σ_1 (Fig. 9, stereoplot 1a). This relationship suggests that N–S compression and E–W extension are closely linked and reveals stress variation from south (where compression prevails near the Himalayan Front) to north (where extension dominates in the Tibet Plateau), as indicated by the geographical distribution of focal mechanism solutions in Bhutan Himalaya (Fig. 9, subzone 1).

In the subzone of Mishmi Thrust (3), N–S compression and N–S extension coexist (Fig. 9, stereoplots 3a and 3b, respectively), which reflects another type of stress permutation between extreme stress axes σ_1 and σ_3. The central subzone of Arunachal Himalaya (2) allowed determination of a single type of stress, but earthquake data are absent in the northern part, and two unclassified mechanisms are compatible with the extensional states of stress identified in adjacent subzones. Other unclassified mechanisms correspond to mechanisms with attitudes or senses of motion incompatible with identified stress states, which may result from the existence of local stress perturbations–permutations or erroneous seismological determinations.

6.3 Northeast India

In the intraplate domain of Northeast India, two distinct states of stress are required to explain the focal mechanism solutions in each subzone (Fig. 10).

In the subzone of Tripura Belt (4), the two compressive stress regimes do not markedly differ, with a difference of only 27° between their trends of σ_1, approximately N–S and NNE–SSW (stereoplots 4a and 4b in Fig. 10). In each of the other two subzones of

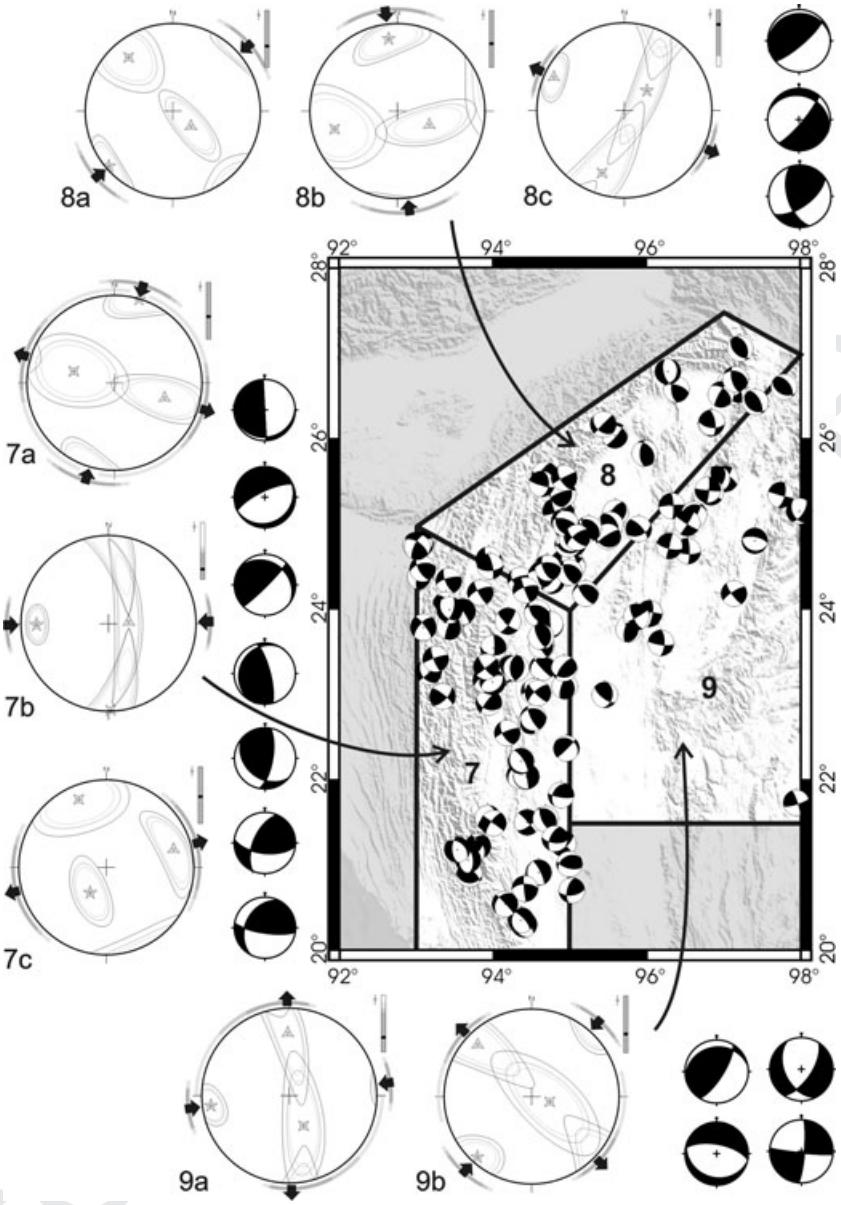

Figure 11. Results of stress inversions coupled with stress separation of focal mechanism solutions for the Indo–Burma Range subsets (7 southern Indo–Burma region, 8 eastern Indo–Burma region and 9 Sagaing Fault region; see Fig. 4 and Table 2). Other explanations as for Fig. 9. See also Table 6.

Shillong Plateau (5) and Assam Valley (6), two contrasting states of stress are reconstructed, with a N–S compression in both cases (stereoplots 5a and 6a, similar to 4a) and a nearly E–W compression with high and low values of Φ consistent with different girdle distributions of confidence ellipses ($\sigma_2 - \sigma_3$ around σ_1 and $\sigma_1 - \sigma_2$ around σ_3: stereoplots 5b and 6b, respectively).

The contrasts between reconstructed stress regimes reveal more complexity of the population of focal mechanism solutions in Northeast India than in Eastern Himalayas. This is not surprising considering the position of Northeast India between two major mountain belt domains, where different seismotectonic regimes prevail. Unclassified mechanisms deserve similar interpretation as before and also include mechanisms compatible with a stress state identified in an adjacent subzone. This may suggest gradual spatial change in seismotectonic stresses, a property that cannot be checked because of the large spatial dispersion of earthquakes.

6.4 Indo–Burma ranges

The most complex distribution of stress states was found in the Indo–Burma Ranges (Fig. 11). To explain the distribution of focal mechanism solutions within reasonable fit levels, three stress regimes are needed in the southern and eastern Indo–Burma regions of the arc (sub-zones 7 and 8, Fig. 11). In contrast, as Fig. 10 shows, two stress regimes account for the seismotectonic behaviour of the foreland domains like the Tripura Belt (sub-zone 4) and the Assam Valley (6).

The simplest separation was done in the southeastern subzone (Sagaing Fault region, 9), which shows the smallest density and variety of focal mechanism solutions. Two major stress regimes occur there, with N–S and NE–SW trends of compression (Fig. 11, stereoplots 9a and 9b, respectively). In both cases, relatively low values of Φ favour permutations between σ_2 and σ_3, as shown by the girdle distribution of the related confidence ellipses (contrasting

with the small size and rounded shape of confidence ellipses around σ_1 axes).

Three states of stress were determined in the southern and eastern subdomains of the Indo–Burma region (subzones 7 and 8, respectively, closer to the mountain front of the Indo–Burma Ranges than subzone 9). However, some geometrical relationships suggest close linkage between at least two of these stress states. In the eastern Indo–Burma region (8), a permutation between all stress axes may account for the difference between stereoplots 8a and 8c (Fig. 11), with low and high values of Φ that account for the girdle distributions of axes $\sigma_2 - \sigma_3$ and $\sigma_1 - \sigma_2$ around tightly constrained axes σ_1 and σ_3 (respectively). The other subset, 8b, reveals a quite different stress state with N–S compression. In the southern Indo–Burma region (7), E–W compression is characterized by a tightly constrained σ_1 axis, with easy permutation between the other two axes, consistent with low Φ ratio and distribution of confidence ellipses for σ_2 and σ_3 (stereoplot 7b in Fig. 11). Despite intermediate values of Φ (revealing triaxial stress with similar differences $\sigma_1 - \sigma_2$ and $\sigma_2 - \sigma_3$), the other two stress states may be related through a permutation between σ_1 and σ_2 (stereoplots 7a and 7c in Fig. 11). Their directions of extension, close to E–W, can be considered as similar, although the trends of σ_3 axes differ by 27°, because the confidence ellipses are rather large. As strike-slip and reverse mechanisms dominate, these two states of stress reflect N–S compression rather than E–W extension. Many unclassified mechanisms can again be explained either by a stress state of an adjacent subzone or by limited rotations that may result from simple uncertainties in the original determinations.

6.5 Multiple stress regimes in Northeast India

The inversion of focal mechanism solutions of earthquakes collected during 57 yr thus reveals multiple but consistent stress states in Northeast India, a large area (nearly 1.5×10^6 km^2) with high structural diversity (Fig. 2). Because higher levels of heterogeneity could be expected considering the large size of subzones, it is remarkable that within a reasonable range of uncertainties, 1–3 states of stress suffice to explain the data in each subzone. Moreover, a comparison between the plunges of stress axes in Fig. 8 (Table 5) and Figs 9–11 (Table 6) shows that a higher proportion of significant plunges are close to horizontal or vertical in the second case, as can be expected in the upper lithosphere. The ratio Φ plays an important role in this geometrical evaluation, because for two principal stresses nearly equal (σ_1 and σ_2 for Φ close to 1, or σ_2 and σ_3 for Φ close to 0), the orientations of the corresponding two axes have little significance. Typical examples of this 'tensor shape effect' occur in steroplots 4b and 5a of Fig. 9 (nearly horizontal σ_1 with low Φ) and steroplot 8c of Fig. 9 (horizontal σ_3 with high Φ).

7 SEISMOTECTONIC REGIMES AS A FUNCTION OF DEPTH: SUBDUCTION BENEATH INDO–BURMA RANGES

Why does significant compression occur in the northern, NE–SW trending segment of the Indo–Burma Ranges (Fig. 11)? The southward movement of the Sunda plate with respect to India should involve opening across the northern Indo–Burma Ranges, not contraction. Not only do compressive focal mechanisms of earthquakes prevail in this belt segment of the northern Indo–Burma Ranges (sub-zone 8 in Table 6 and Fig. 11), but also the presence of recent folds and thrusts implies belt-perpendicular contraction in addition to right-lateral strike-slip. Another major feature is the presence of a descending slab of Indian lithosphere beneath the Burmese arc as an onshore extension of the Andaman subduction zone. Before examining the relationships between seismotectonic stresses and plate kinematics, it is necessary to analyse the distribution of earthquake mechanisms and related stress regimes as a function of depth in the entire domain of the Indo–Burma Ranges (Fig. 12).

In the stress reconstructions of the previous sections, no separation according to depth was shown because all earthquakes used have occurred in the upper lithosphere, and differences as a function of depth were not paramount. Earthquakes deeper than 90 km

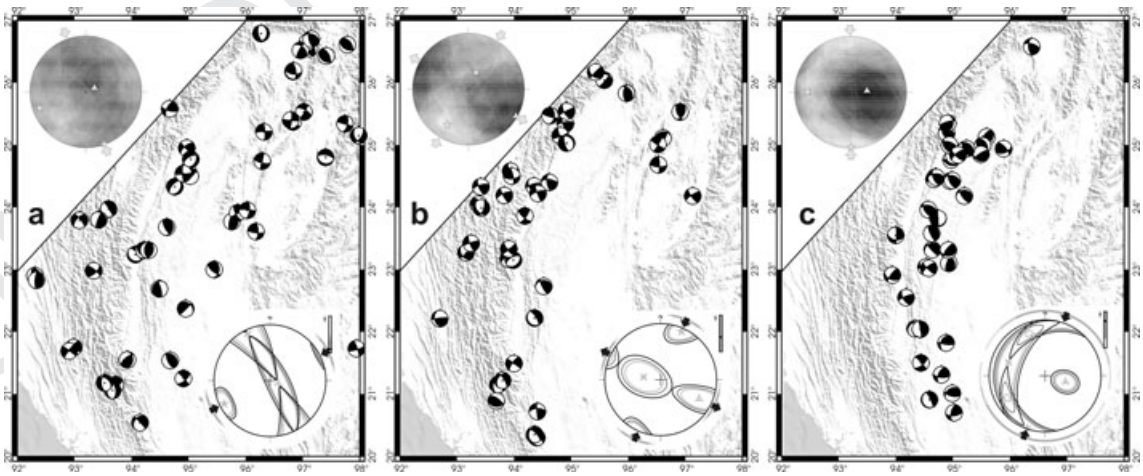

Figure 12. Map of focal mechanism solutions in the Indo–Burma Ranges. The three maps correspond to different earthquake depth ranges in the same area: (a) 0–45 km; (b) 45–90 km and (c) 90–160 km. Focal mechanism solutions shown as 'beachballs' (caption as for Fig. 4). For right-dihedra analysis (stereoplots in upper-left-hand corner of maps), caption as for Fig. 6. Right-hand dihedra stereoplots refer to complete data subsets: (a) 56 focal mechanism solutions above 45 km depth with compatibility levels 65 per cent for pressure and 57 per cent for tension; (b) 39 solutions from 45 to 90 km depth with compatibility levels 85 per cent for pressure and 79 per cent for tension and (c) 38 solutions deeper than 90 km with compatibility level 89 per cent for pressure and 95 per cent for tension. For stress inversion (stereoplots in lower-right corners of maps), caption as for Fig. 8. Refining process as explained in Section 4 of text, giving (a) 49 per cent of data acceptable with average fit $\omega = 75$ per cent ($\omega_{acc} = 45$ per cent), (b) 54 per cent of data acceptable with average fit $\omega = 79$ per cent ($\omega_{acc} = 50$ per cent) and (c) 79 per cent of data acceptable with average fit $\omega = 77$ per cent ($\omega_{acc} = 45$ per cent).

only occur beneath the Indo–Burma Ranges, with depths down to 160 km (Fig. 3c). We consequently examined how mechanisms vary as a function of depth in a quadrangle from 20°N to 27°N in latitude and 92°E to 98°E in longitude (Fig. 12). The focal mechanism solutions located near the northwest corner were discarded because they do not belong to the Indo–Burma Ranges; two earthquakes deeper then 90 km were thus ignored. We then separated three depth ranges: 0–45; 45–90 and 90–160 km. The earthquakes shallower than 45 km show large dispersion of epicentres (Fig. 12a). For deeper earthquakes, a simple comparison between epicentre distributions in maps highlights the eastward deepening, consistent with the eastward dip and southward development of the subduction zone (*cf.*Figs 12b and c).

The pressure–tension distribution for each entire subset reveals trends of compressions around N–S (NNW–SSE to NNE–SSW, see the right dihedra stereoplots in Fig. 12). The maximum probability obtained for pressure and tension remarkably increases with depth, from 61 per cent on average for earthquakes shallower than 45 km to 92 per cent for earthquakes deeper than 90 km (see the caption of Fig. 12). In terms of stress, this variation reveals a typical transition from heterogeneity in the upper lithosphere (for shallow earthquakes, in agreement with the results presented in Table 6 and Fig. 11) to relative homogeneity at larger depths.

The stress inversion has been done for the three depth-based subsets of Fig. 12. In each case, the refining process allows determination of a stress regime using reasonable threshold values ($\omega_{acc} = 45$–50 per cent). The dominating stress regime varies with depth, from ENE–WSW compression above 45 km depth to NNE–SSW compression for earthquakes deeper than 45 km. The proportion of acceptable mechanisms increases with depth, from 49 to 79 per cent. A single stress regime, thus, accounts for earthquakes deeper than 90 km, which is not the case at shallow depths. As the NNE–SSW compression is poorly represented in the upper lithosphere (Fig. 12a) whereas it is the single major regime at depth (Fig. 12c), a plausible origin of this compression beneath the Indo–Burma Ranges is the pressure exerted on the dipping slab by both its eastward-concave bending that induces arc-parallel contraction in the lithosphere and the regional N–S compression.

8 DISCUSSION AND CONCLUSIONS

8.1 Synthesis of palaeostress results

The nine subzones analysed in Sections 3–5 of this paper were designed as a function of the pattern of major structural units and the need for a sufficient number of focal mechanism solutions in stress inversion (Section 4) and inversion-separation (Section 5). Had the subzones been more numerous and hence smaller, some stress states would not have been reliably defined. Had these subzones been larger, significant variations in seismotectonic stress along and across major structural units would have been ignored. The stress variation with depth in the Indo–Burma Ranges was also considered (Section 6). Table 7 and Fig. 13 provide a synthetic view of our stress results for comparison with the present-day kinematic data in a further subsection.

The N–S compression is represented in all subzones except the Sagaing Fault Region (9). It corresponds to the largest mechanically homogeneous subset in each major domain (Eastern Himalayas, Northeast India and Indo–Burma Ranges). This N–S compression, I in Table 7, is related to the N–S convergence between India and Eurasia, although it may also locally result from the eastward concave bending of the northern Indo–Burma arc, as pointed out in Section 6. The largest fault structures related to this N–S compression are the MCT and MBT in Eastern Himalaya, but also the Dauki Fault and the Brahmaputra Fault that bound the Shillong Plateau pop-up structure in the northeast Indian plate (Fig. 13a).

From an analysis of borehole breakouts and focal mechanism solutions, Gowd *et al.* (1992) found a NNE–SSW (N23°E) compression. The 25° deviation from the σ_1 trend that we obtained (N2°W ± 14°, Table 7) is partly explained by the larger size of their study area and a lower data density. In addition, we identify a distinct, NE–SW compression in the Indo–Burma Ranges, which they included in their azimuthal average. The single-event focal mechanism solutions in the World Stress Map are consistent with N–S compression along the Himalayan Front in Northeast India and E–W extension in the Tibetan Plateau (Heidbach *et al.* 2005, 2007). The World Stress Map also indicates that the N–S compression

Table 7. Synthesis of the stress inversions results of Table 6 and Figs. 9–11.

Domain	Stress state	Regime	Subzones	N	Az	Φ	Type
Eastern Himalayas	N–S compression	I	1a, 2, 3a	39	163 ± 16	0.38	r + ss
	E–W extension	I (^{1})	1b	22	92 ± 17	0.59	n
	N–S extension	I (^{2})	3b	5	178 ± 30	0.44	n
Northeast India	N–S compression	I	4a, 5a, 6a	32	6 ± 6	0.32	ss
	E–W compression	II	5b, 6b	18	100 ± 20	0.41	ss
	NE–SW compression	III	4b	12	34 ±14	0.06	ss + r
Indo–Burma Ranges	N–S compression	I (*)	7a, 8b	36	6 ±18	0.41	ss + r
	E–W compression	II	7b, 9a	20	267 ± 6	0.21	r + ss
	E–W extension	II (^{2})	7c, 8c	27	85 ±17	0.54	n
	NE–SW compression	III	8a, 9b	30	227 ±14	0.36	r + ss

Note: Three major seismotectonic stress regimes are numbered I, II and III. Regime I is related to India–Eurasia convergence. Regime II is related to convergence between outer Indo–Burma Ranges and Indian plate. Regime III is related to convergence between Sunda plate and inner Indo–Burma Ranges and possibly to lateral escape of Shillong block and plate interaction near Assam Syntaxis.

Exponents between parentheses refer to subregimes resulting from permutations between σ_2 and σ_3 (^{1}) or σ_1 and σ_3 (^{2}), or indicate compression involving deep earthquakes (*) beneath the Indo–Burma Ranges (Fig. 12). Subzones have the same reference numbers as before.

N, number of focal mechanism solutions; Az, weighted average azimuth of compression or extension (according to stress state), in degrees; Φ, weighted average ratio of principal stress differences; Type, dominating type of focal mechanism solutions (r reverse, ss strike-slip, n normal).

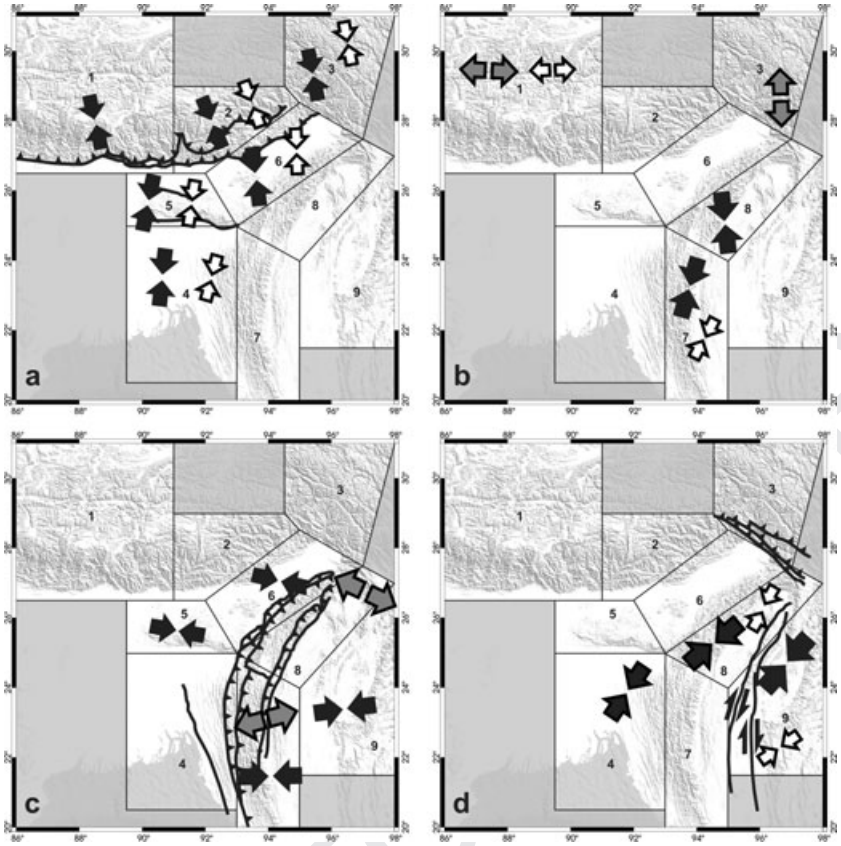

Figure 13. Synthesis of main stress regimes. Subzones 1–9 as in previous figures and tables. Pairs of convergent arrows for compression, divergent arrows for extension. Small open arrows indicate the average stress regime in each subzone (from Table 5 and Fig. 8). Large arrows (black for compression, grey for extension) refer to final determinations (from Tables 6 and 7 and Figs 9–11). Four types of seismotectonic stress regimes account for 85 per cent of our total data set: (a) major N–S compression related to India–Eurasia convergence; (b) subsidiary extensional regimes related to India–Eurasia convergence, also N–S compression indicated by deepest earthquakes below Indo–Burma Ranges (Fig. 12). (a) and (b) are referred to as regime I (N–S compression) in Table 7. (c) E–W compression related to convergence between outer Indo–Burma Ranges and Indian plate, and subsidiary arc-perpendicular extension in Burmese arc, referred to as regime II in Table 7. (d) NE–SW compression related to convergence between Sunda plate and inner Indo–Burma Ranges and plate convergence interaction near the Assam Syntaxis, referred to as regime III in Table 7. Some major structures activated by the main compressive stress regimes are added (see Fig. 2 for details): Main Central Thrust and Main Boundary Thrust of Eastern Himalaya; Dauki Fault and Brahmaputra Fault of Shillong Plateau in (a); front fault of Tripura Belt; Naga, Disang and other thrusts of outer Burmese arc; Eastern Boundary Thrust of Indo–Burma Ranges in (c), major strike-slip faults of Myanmar Central Basins and Sagaing Fault as well as Mishmi–Lohit Thrusts of the Assam Syntaxis in (d).

extends to the south into the Shillong Massif and the Bengal Basin regions, in agreement with our results (Fig. 13a).

Not only does this stress regime of N–S compression dominate, it is also closely related to particular subregimes (Fig. 13b) such as E–W extension (through permutation between σ_1 and σ_2, compare 1a and 1b in Fig. 9) and N–S extension (permutation between σ_1 and σ_3, compare 3a and 3b in Fig. 9). The first type of permutation is related to transition from reverse and strike-slip faulting to normal faulting (Angelier & Bergerat 1983; Hu & Angelier 2004). The second type of permutation involves belt-perpendicular dilation in arcs, where slab pull and upward-convex bending occur, and mountain belts experiencing deviatoric stress of gravitational origin. The deepest earthquakes beneath the Indo–Burma Ranges also reveal N–S compression (Fig. 12 and Fig. 13b), related to SE-concave horizontal bending of the slab and not resulting from India–Eurasia convergence in a direct way.

In Northeast India and Indo–Indo-Burma Ranges, E–W compression occurs in four sub sub-zones (5, 6, 7 and 9, Fig. 13c). This compression, II in Table 7, is absent in the Eastern Himalayas. It results from the convergence across the front zones and foreland of the Indo–Indo-Burma Ranges. The largest fault structures activated by this compression are the front of the Tripura Belt, the thrusts of the outer Burmese arc and the Eastern Boundary Thrust in the Indo–Indo-Burma Ranges (Fig. 13c). As discussed later, the E–W compression in the sub sub-zones of Shillong Plateau (4) and Assam Valley (6) could well be related to the eastward lateral extrusion of a block of Indian lithosphere.

The nearly E–W extension in sub sub-zones 7 and 8 of the Burmese arc (Fig. 13c) is a probable expression of belt-perpendicular dilation (inducing permutation between $\sigma 1$ and σ_3), as a result of underlying slab pull-retreat and upward-convex bending in the subducting plate. Local relation to the widespread N–S compression (through $\sigma_1 - \sigma_2$ permutation as in Bhutan Himalaya) cannot be excluded. However, the clockwise change in the direction of extension from south to north along the Indo–Burma Ranges (ENE–WSW in subzone 7, ESE–WNW in subzone 8: Fig. 13c) accompanies the change in arc trend. Moreover, among the 27 normal-type earthquakes indicating E–W extension, 13 are located at depths larger than 60 km. The E–W extension in the outer Indo–Burma Ranges is consequently attributed to regime II in Table 7 and reflects subduction-related, arc-perpendicular extension within the frame of arc-foreland convergence in a nearly E–W direction.

A NE–SW compression (Fig. 13d) is clearly identified in the northern Indo–Burma Ranges (eastern Indo–Burma region, 8, and Sagaing Fault region, 9) and locally in their Indian plate foreland (Tripura Belt, 4). This regime, III in Table 7, involves belt- parallel compression in the NE–SW trending segment of the northernmost Indo–Burma Ranges (eastern Indo–Burma region, 8). This compression also affects the Indian foreland close to the major structural bend of the Indo–Burma Ranges (northern portion of Tripura Belt, 4), as well as their inner zones (northern half of Sagaing Fault region, 9). The NE–SW compression results from plate convergence interaction between Eurasia, India, Burma and Sunda. It is consistent with the presence of major right-lateral strike-slip that trend N–S east of the Myanmar Central Basins, especially, the Sagaing Fault; it is also consistent with the Mishmi and Lohit thrusts of the Assam Syntaxis (Fig. 13d).

8.2 Comparison with other sources and methodological insights

Gowd *et al.* (1992) identified E–W compression and N0–30°E compression from borehole breakouts and focal mechanism solutions. The World Stress Map also indicates E–W compression from single event focal mechanisms solutions in the foreland of the Indo–Burma Ranges between the Tripura Belt and the Shillong Massif, compatible with borehole breakouts in the Bengal Basin (Heidbach *et al.* 2005, 2007). Also, the N26°E azimuth of maximum stress determined by Gahalaut & Gahalaut (2007) based on stress inversion of focal mechanism solutions of earthquakes is partly compatible with some trends of σ_1 that we determined in the Tripura Belt and the southern and eastern Indo–Burma region (sub-zones 4, 7 and 8; Table 5 and Fig. 8).

Stress inversion indicated that within the range of uncertainties in focal mechanism determinations, the stress regimes are inhomogeneous. The N26°E compression probably results from averaging between two or three mixed stress regimes with different trends of compression (Fig. 13). Reliable determination of seismotectonic stress requires (1) inversion of as many focal mechanism solutions as possible instead of consideration of single-event data and (2) where geodynamic setting is complex, separation of two or more stress states compatible with reasonable fit levels that depend on technical data uncertainties and natural dispersion.

The seismotectonic regimes in the studied area involve three major compressions, including subsidiary states of stress resulting from permutations between principal axes (Table 7). The regime I related to India–Eurasia convergence is widespread and documented by 134 focal mechanism solutions, that is 47 per cent of the data (including 25 per cent for typical N–S compression between and inside convergent plates, 9 per cent for subsidiary extensions and 13 per cent for intraslab deformation at depth). The regime II related to outer Burmese arc-India convergence and partly to possible extrusion of the Shillong block is consistent with 65 focal mechanism solutions (23 per cent of the data including 13 per cent for typical E–W compression in Northeast India and Indo–Burma Ranges and 10 per cent for subsidiary E–W extension in the outer Burmese arc). The regime III, as revealed by 15 per cent of the data, results from plate interaction in the Assam Syntaxis area and the eastern Indo–Burma Ranges. The remaining 15 per cent of the data (44 unclassified focal mechanism solutions shown as beachballs in Figs 9, 10, 11) correspond to three situations: (1) solutions poorly represented in the subzone considered but compatible with a stress regime present in an adjacent subzone; (2) local stress situations without regional significance and (3) possible presence of wrong focal mechanism solutions.

8.3 Relation to plate kinematics: partitioning across the Indo–Burma Ranges

Discussing the plate kinematics in terms of poles of rotation and geodetic data is beyond the scope of this paper. To present the major kinematic features in a simple way (Fig. 14), we rely on many recent analyses, which in the first approximation reveal a general kinematic agreement in the study area (Bilham & Gaur 2000, Jouanne *et al.* 2004, Socquet *et al.* 2006, Gahalaut & Gahalaut 2007, Jade *et al.* 2007). For details, the reader is referred to these published analyses, in which the GPS stations and their displacement vectors are listed.

According to Socquet *et al.* (2006), the motion of the Sunda Plate with respect to India is about 35 mm yr^{-1} in the SSW direction in Myanmar near latitude 22°N. In the same region, Gahalaut & Gahalaut (2007) calculated the motion of the Sunda plate relative to the Burma backarc domain and the motion of this backarc domain relative to India. Their determinations resemble the previous ones in terms of rates but differ in terms of directions. Assuming that the present-day displacement between Burma and India is compatible with the recent fold-and-thrust structure in the northernmost segment of the Burmese arc, the velocity vectors from Socquet *et al.* (2006) show better compatibility with the tectonic framework in the studied area.

In any case, taken alone a SSW- or SW-directed displacement of Burma with respect to India hardly explains the belt perpendicular contraction across the NE–SW trending northern segment of the Indo–Burma Ranges. The regional kinematics also imply decoupling across Indo–Burma Ranges, especially along N–S trending right-lateral strike-slip faults, such as the Sagaing Fault (between Sunda Plate and backarc domain) and the Kabaw Fault (between backarc domain and Burma arc). We infer that between the Indo–Burma Ranges and Northeast India, partitioning occurs and involves a large difference in azimuth between thrust-type contraction at range front and right-lateral transpression in the innermost domains of the arc.

To illustrate the kinematics of the studied region, we adopted a reference frame attached to Lhasa, Tibet (velocities as large open arrows in Fig. 14). Northeast India shows a northward displacement of 14–15 mm yr^{-1} with respect to Lhasa (arrow 3 in Fig. 14), according to GPS measurements over nearly 10 yr (Jouanne *et al.* 2004, see also Jade *et al.* 2007). Adopting the displacement of India with respect to Sunda indicated by Socquet *et al.* (2006), one determines an average velocity of about 22–23 mm yr^{-1} toward the southwest for the western edge of the Sunda plate near 22°N, on the eastern side of the Sagaing Fault (arrow 1 in Fig. 14), also with respect to Lhasa. In the same kinematic frame, the average velocity at the same latitude in the western Myanmar Central Basins of the Burma Plate, east of the Kabaw Fault, is about 12 mm yr^{-1} toward the NW (arrow 2 in Fig. 14). The difference between these two velocity vectors, 1 and 2, is about 24 mm yr^{-1} toward the SSW, revealing a large N–S component of belt-parallel slip, nearly 24 mm yr^{-1} in dextral sense and a smaller E–W component of belt-perpendicular shortening, about 6 mm yr^{-1} (arrows b, c and d in Central Myanmar, Fig. 14). Whereas the E–W component indicates limited shortening across Central Myanmar, most of the N–S component is the expression of right-lateral slip of the Sagaing Fault, as evidenced from GPS near this fault (Vigny *et al.* 2003).

The comparison between the displacement of the Myanmar Central Basins and that of the Bengal Basin in eastern India (arrows

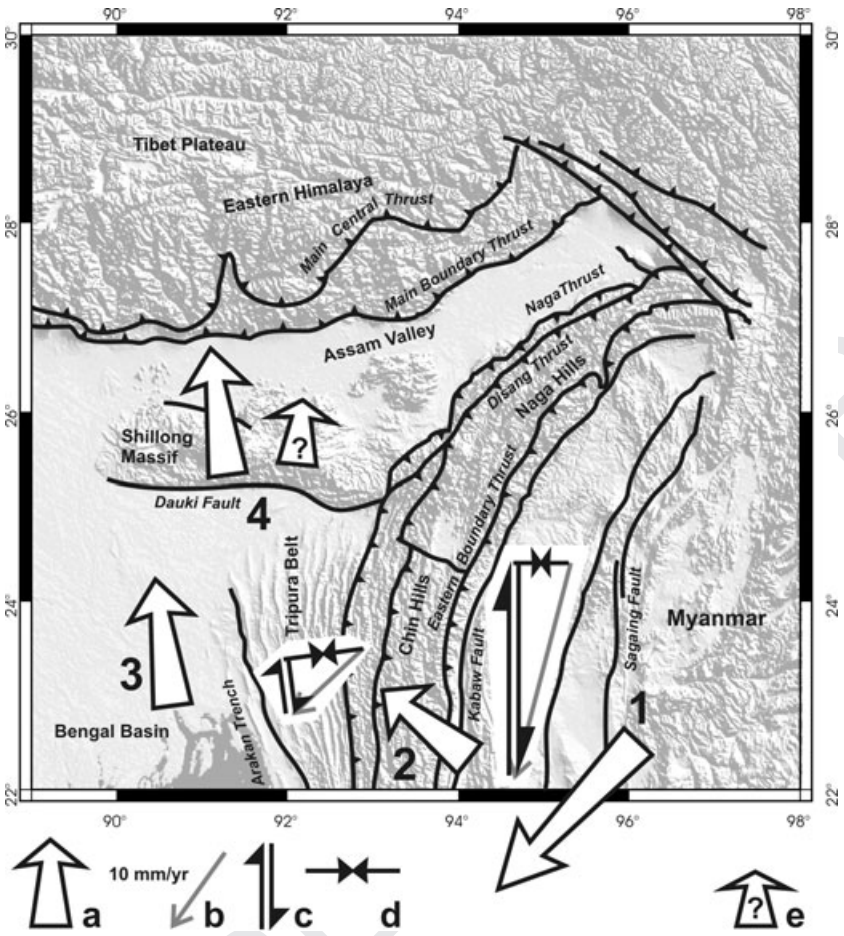

Figure 14. Major kinematic features of Northeast India. (a) Present-day average velocities relative to Lhasa, Tibet: 1 western edge of Sunda plate; 2 Central Myanmar basins; 3 Bengal Basin; 4 Shillong–Mikir Massif. (b) To the east, velocity of 1 with respect to 2, mainly accommodated along Sagaing Fault; to the west, velocity of 2 with respect to 3 accommodated across various faults of the Burmese Arc and Tripura Belt. (c) Right-lateral strike-slip, belt-parallel component of (b). (d) Shortening, belt-perpendicular component of (b). Symbols (a), (b), (c) and (d) at the same scale (10 mm yr^{-1}). (e) Inferred recent average velocity of the Shillong–Mikir Massif with respect to Lhasa, smaller than 4 but not at scale.

2 and 3 respectively in Fig. 14) shows a different pattern of relative displacement. The difference vector, about 11 mm yr^{-1} toward the SW, reveals a N–S component of belt-parallel slip, about 6 mm yr^{-1} in dextral sense, smaller than the E–W component of belt-perpendicular shortening, about 9 mm yr^{-1} (arrows b, c and d in western Indo–Burma Ranges and Tripura Belt, Fig. 14). Although the distribution of present-day displacements is still poorly documented because permanent GPS stations are few, this comparison reveals partitioning across the Indo–Burma Ranges. In the inner belt, dextral strike-slip in the N–S direction prevails, mainly accommodated along the Sagaing Fault. In the outer belt, dextral strike-slip is less and across-belt shortening dominates. Combining velocity vectors 1 and 3 in Fig. 14, one obtains a velocity of about 35 mm yr^{-1} in the S28°W direction, that is, the SSW-directed motion of the western edge of the Sunda Plate with respect to India near 22°N.

Most of the belt-parallel right-lateral slip is probably accommodated between the Sagaing Fault (inclusively) and the western edge of the Myanmar Central Basins, whereas belt-perpendicular shortening predominates in the outer Indo–Burma Ranges and the Bengal Basin foreland belt (compare in Fig. 14 the components c and d of the two relative velocities b). This expected distribution would account for the fan-shaped distribution of folds in the Tripura Belt, with N–S axes to the east and NNW–SSE ones to the west. In contrast with the N–S trends of the inner belt, inherited from earlier tectonic events, the most recent folds and reverse faults, close to the Bengal Basin, probably tend to develop perpendicular to ENE–WSW shortening that prevails in this foreland region of the Burmese Arc. The present-day velocity distribution across the arc is thus in agreement with the probable recent tectonic evolution in the belt front zone.

8.4 Kinematics of the Shillong–Mikir–Assam Valley block

Regarding the displacement of India with respect to Tibet (arrow 3 in Fig. 14), the geological evidence of N–S shortening across the Shillong Plateau and the front thrusts of the Himalayas, supported by the existence of large earthquakes such as the Great Assam earthquake of 1897, apparently conflicts with the recent GPS data. These data revealed the absence of N–S deformation between the southern Shillong Plateau and the Brahmaputra Valley (Jade *et al.* 2007). For this reason, Fig. 14 shows identical velocity for 3 (Bengal Basin) and 4 (Shillong Plateau and Assam Valley) in the Lhasa-attached frame. This apparent contradiction indicates that the northeastern portion of the Indian Plate, instead of being stable or subject to aseismic creep, is in a temporary locked situation. Whereas the

instantaneous velocities with respect to Tibet are almost identical for the Indian craton and the block including the Shillong–Mikir massifs and the Assam Valley, over a medium-term time range (e.g. the Late Pleistocene-Holocene), we propose a significantly lower velocity for this block with respect to Tibet (arrow e, without scale, in Fig. 4).

This conclusion is consistent with the convincing interpretation of the Shillong Plateau as a giant pop-up structure presented by Bilham & England (2001). Most of the shortening between Indian craton and the Shillong block is expected to occur on the reverse Dauki Fault. This kinematic behaviour of the Shillong block in the broad sense (including Mikir Plateau and Assam Valley) is consistent with the dominating N–S compression revealed by our inversions of focal mechanism solutions in the Shillong Plateau (5) and Assam Valley (6) subzones (Fig. 13a). However, our inversions also revealed significant E–W compression in the same subzones (Fig. 13c), and some focal mechanisms involve a possible component of right-lateral strike-slip on the major E–W block-bounding faults. In addition to separation from India across major reverse faults, eastward extrusion of the entire Shillong–Mikir–Assam Valley block towards the Assam Syntaxis, at the northeast corner of the Indian plate, deserves consideration. The relative importance of N–S contraction and eastward escape is unknown (a minor strike-slip component is assumed in Fig. 14), as a target for seismotectonic studies along and around the Dauki Fault.

8.5 Consistency between seismotectonic stress and kinematics

Although the present-day pattern of regional stresses reconstructed based on the inversion of focal mechanism solutions of earthquakes (Fig. 13) and the kinematic reconstruction supported by consideration of regional structure and geodetic data (Fig. 14) radically differ in nature and origin, their comparison reveals high levels of consistency.

The widespread N–S compressive stress (Fig. 13a) is perfectly consistent with the northward displacement of India with respect to Tibet (Fig. 14). This compression is clearly evidenced by focal mechanism solutions of relatively large earthquakes inside the north-eastern portion of the Indian plate, including the Bengal Basin, the Shillong–Mikir Massif and the Assam Valley (sub-zones 4–5–6 in Fig. 13a), in excellent agreement with the N–S shortening between these regions and the Indian craton (arrows 4 in Fig. 14).

The northeastern corner of the Indian plate also undergoes significant E–W compression (subzones 5–6 in Fig. 13c), suggesting eastward extrusion of a Shillong–Mikir–Assam Valley block and shortening in the E–W direction with respect to the northern Indo–Burma Ranges. Considered alone, the SW-directed motion of the so-called Burma plate with respect to India (Fig. 14, grey arrow between 2 and 3) would fail to account for the occurrence of compression in both the N–S and E–W directions in the upper Assam Valley (Fig. 13 a and b respectively, subzones 5 and 6). The hypothesis of block extrusion provides solution of this kinematic problem and well accounts for the regional stress distribution.

As a particular subduction-related feature, the N–S compression that affects the outer zones of the Indo–Burma Ranges in the southern and eastern regions (subzones 7 and 8, respectively; Fig. 13a) is principally related to earthquakes at depth, in the descending slab of the Indian lithosphere. It reflects arc-parallel shortening in the slab, related to the increasing bending of the northernmost Burmese arc. Thus, its relation to the India–Eurasia convergence is not direct, although the N–S convergence certainly favours horizontal bending in the northern Burmese arc.

Compared with the effects of the India–Eurasia collision in the Himlayas, the stress and velocity patterns in the Indo–Burma Ranges reveal higher levels of complexity. Two aspects—the occurrence of N–S compression at depth in and around the descending slab and the existence of arc-perpendicular extension indicated by shallower earthquakes (Fig. 13c, subzones 7 and 8)—are related to the subduction of the Indian plate beneath Burma. The first aspect is discussed above; the second aspect is a classical feature in many arcs above subduction zones.

The remaining stress states in the Indo–Burma Ranges, which are major, reveal a NE–SW trending compression that affects the northeastern segment and inner zones of the Burmese arc (Fig. 13d), turning to an E–W compression in the southern segment and outer zones (Fig. 13c). Both these directions of compression are present in the southeastern region that belongs to the Burma and Sunda plates. This distribution of maximum stress indicated by earthquake focal mechanism solutions is consistent with the distribution of relative displacement across the Indo–Burma Ranges, showing an evolution from SSW trends in the inner zones to WSW ones in the outer zones (Fig. 14b, arrows b). A clockwise change of about 45° thus affects both the maximum compressive stress and the displacement, in agreement with the interpretation in terms of stress–strain partitioning across the Indo–Burma Ranges. Also consistent with partitioning, the direction of maximum stress shows systematic clockwise deviation compared with the direction of relative displacement (NNE–SSW displacement and NE–SW maximum stress in the inner domains; ENE–WSW displacement and E–W maximum stress in the outer ones).

ACKNOWLEDGMENTS

The research was supported by the North-East Institute of Science and Technology (Assam, India) for establishing the database of focal mechanism solutions and the Institut Universitaire de France (IUF) for stress analysis. Constructive comments by two referees, Mark Tingay and Agust Gudmundsson, and the Editor, Saskia Goes, led to significant improvement of the manuscript. They are all gratefully acknowledged.

REFERENCES

Angelier, J., 1975. Sur l'analyse de mesures recueillies dans des sites faillés: l'utilité d'une confrontation entre les méthodes dynamiques et cinématiques, *C. R. Acad. Sci. Paris, D*, **281,** 1805–1808 [Erratum: Ibid., (D), 283, 1976, p. 466].

Angelier, J., 1984. Tectonic analysis of fault slip data sets, *J. geophys. Res.*, **89,** 5835–5848.

Angelier, J., 1989. From orientation to magnitudes in paleostress determinations using fault slip data, *J. Struct. Geol.*, **11**(1/2), 37–50.

Angelier, J., 1990. Inversion of field data in fault tectonics to obtain the regional stress, III: a new rapid direct inversion method by analytical means, *Geophys. J. Int.*, **103,** 363–376.

Angelier, J., 2002. Inversion of earthquake focal mechanisms to obtain the seismotectonic stress, IV: a new method free of choice among nodal planes, *Geophys. J. Int.*, **150,** 588–609.

Angelier, J. & Bergerat, F., 1983. Systèmes de contrainte et extension intracontinentale. Colloque "Rifts et Fossés Anciens", *Marseille. Bull. Centr. Rech. Expl.-Prod. ELF-Aquitaine*, **7,** 137–147.

Angelier, J. & Mechler, P., 1977. Sur une méthode graphique de recherche des contraintes principales également utilisable en tectonique et en séismologie: la méthode des dièdres droits, *Bull. de la Société Géologique de France*, **7,** 1309–1318.

Angelier J., Slunga, R.F., Bergerat, F., Stefansson, R. & Homberg, C., 2004. Perturbation of stress and oceanic rift extension across transform faults shown by earthquake focal mechanisms in Iceland, *Earth planet. Sci. Lett.*, **219,** 271–284.

Angelier, J., Bergerat, F., Stefansson, R. & Bellou, M., 2008. Seismotectonics of a newly formed transform zone near a hot spot: earthquake mechanisms and regional stress in the South Iceland Seismic Zone, *Tectonophysics*, **447,** 95–116, doi:10.1016/j.tecto.2006.07.016.

Annual Seismological Bulletin, 1982–2006.Geoscience Division, *Res. Lab. Jorhat (CSIR) Ed.*,Vol.1–15, pp. 1–1386, published jointly by Regional Research Laboratory, Jorhat, and National Geophysical Research Institute, Hyderabad.

Baruah, S., Duarah, R. & Yadav, D.K., 1997. Pattern of seismicity in Shillong Mikir plateau and the orientation of compressional axis, *J. Geol. Soc. Ind.*, **49,** 533–538.

Baruah, S., Hazarika, D., Kayal, J.R., Gogoi, N.K., Duarah, R., Bora, P.K. & Mukhopadyay, S., 2007. Seismotectonics and current state of stress in Chedrang valley and its vicinity—the rupture area of great Assam earthquake of June 12, 1897 (M = 8.7) from waveform and stress tensor inversion, *Geophys. Res. (Abstracts)*, **9**, 00127, Sref-ID 1607–7962/gra/EGU2007-A-00127.

Bilham, R., 2006. *Comment on "Interpreting the style of faulting and paleoseismicity associated with the 1897 Shillong, northeast India, earthquake" by C.P. Rajendran et al.*, *Tectonics*, **25,** TC2001, doi:10.1029/2005TC001893.

Bilham, R. & England, P., 2001. Plateau pop-up during the great 1897 Assam earthquake, *Nature*, **410,** 806–809.

Bilham, R. & Gaur, V.K., 2000. The geodetic contribution to Indian seismotectonics, *Cur. Sci.*, **79**(9), 1259–1269.

Bott, M.H.P., 1959. The mechanisms of oblique slip faulting, *Geol. Mag.*, **96,** 109–117.

Bouchon, M., 1981. A simple method to calculate Green's functions for elastic layered media, *Bull .seism. Soc.Am.*, **71,** 959–971.

Brunnschweiler R.O., 1966. On the geology of the Indo-Burman ranges (Arakan Coast and Yoma, Chin Hills, Naga Hills), *Geol. Soc. Aus. J.*, **13**(1), 137–194.

Carey, E. & Brunier, B., 1974. Analyse théorique et numérique d'un modèle mécanique élémentaire appliqué à l'étude d'une population de failles, *C. R. Acad. Sc., Paris, D*, **279,** 891–894.

Chandra, U., 1984. Seismicity, earthquake mechanisms, and tectonics of Burma, 20°–28°N, *Geophys. J.R. astr. Soc*., **40,** 367–381.

Chen, W.P. & Molnar, P., 1990, Source parameters of earthquakes and intraplate deformation beneath the Shillong plateau and the northern ranges, *J. geophys. Res.*, **95,** 12 527–12 552.

Coutant, O., 1989. Programme de simulation numérique AXITRA. Res. Report LGIT, Grenoble, France, 1989.

Curray, J.R., Moore, D.G., Lawver, L.A., Emmel, F.J., Raitt, R.W., Henry, M. & Kieckhefer R., 1979. Tectonics of the Andaman Sea and Burma, in *Geological and Geophysical Investigations of Continental Margins*,Vol. 29, pp. 189–198, eds Watkins, J.S., Montadert, L. and Dickenson P., *American Association of Petrochemical Geology Memoir*.

Curray, J.R., Emmel, F.J., Moore, D.G. & Raitt, R.W., 1982. Structure, tectonics, and geological history of the northeastern Indian Ocean, in *The Ocean Basins and Margins-The Indian Ocean*,Vol. 6, eds, Nairn, A.E. and Stehli, F.G., Plenum, New York, pp. 399–450.

Das, S. & Filson, J.R., 1975. Tectonics of Asia, *Earth planet. Sci. Lett.* **28,** 241–253.

Das Gupta, S. & Nandy, D.R., 1982. Seismicity and tectonics of Shillong plateau, NE India in *Proceedings of the VII Symposium on Earthquake Engineering*, Univ. of Roorkee, **1,** 19–24.

Dasgupta, S., Mukhopadhyay, M., Bhattacharya, A. & Jana, T.K., 2003, The geometry of the Burma–Andaman subducting lithosphere, *J. Seism.*, **7,** 155 – 174.

Dziewonski, A.M. & Woodhouse, J.H., 1983. An experiment in the systematic study of global seismicity: centroid-moment tensor solutions for 201 moderate and large earthquakes of 1981, *J. geophys. Res.*, **88**: 3247–3271.

Dziewonski, A.M., Chou, T.-A. & Woodhouse, J.H., 1981. Determination of earthquake source parameters from waveform data for studies of global and regional seismicity, *J. geophys. Res.,* **86**: 2825–2852.

Evans, P., 1964. The tectonic framework of Assam, *J. Geol. Soc. Ind.*, **5,** 80–96.

Gahalaut, V.K. & Gahalaut, K., 2007. Burma plate motion, *J. geophys. Res.,* **112,** B10402, doi:10.1029/2007JB004928.

Gansser, A., 1964. *Geology of Himalayas*. Inter Science, London, 289 pp.

Gowd, T.N., Srirama Rao, S.V. & Gaur, V.K. 1992. Tectonic stress field in the Indian subcontinent, *J. geophys. Res.*, **97,** B8, 11 879–11 888.

Gupta, H.K., Singh, S.C., Dutta, T.K. & Saikia, M.M., 1984. Recent investigations of North East India seismicity, in *Proceedings of the International Symposium on Continental Seismicity and Earthquake Prediction*, eds Go G. & Ma X.-Y., Seismological Press, Beijing, pp. 63–71.

Heidbach, O., Fuchs, K., Müller, B., Reinecker, J., Sperner, B., Tingay, M. & Wenzel, F., 2005. World Stress Map, Release 2005, Commission de la Carte géologique du Monde, Paris, and Heidelberg Academy of Sciences and Humanities, 1 sheet (see also 2008 update by Heidbach, O., Tingay, M., Barth, A., Reinecker, J., Kurfeß, D., and Müller, B. '*the 2008 release of the World Stress Map*' available at www.world-stress-map.org).

Heidbach O., Fuchs K., Muller B., Reinecker J., Sperner B., Tingay M. & Wenzel F. 2007. The world stress map, *Episodes*, **30,** 197–201.

Hu, J.-C. & Angelier, J., 2004. Stress permutations: three-dimensional distinct element analysis accounts for a common phenomenon in brittle tectonics, *J. geophy. Res.*, **109,** B09403, doi:10.1029/2003JB002616, 2004, 20 pp.

Husson, L., Mugnier, J.-L., Leturmy, P. & G. Vidal, 2004, Kinematics and sedimentary balance of the Sub-Himalayan Zone, western Nepal, in *Thrust tectonics and hydrocarbon systems*,Vol. **82**, pp. 115– 130, ed. McClay K.R., AAPG Memoir.

Jade, S. *et al*., 2007. Estimates of interseismic deformation in Northeast India from GPS measurements, *Earth planet. Sci. Lett.*, **263,** 221–234.

Jouanne, F. *et al*., 2004. Current shortening across the Himalayas of Nepal, *Int. J. Geophys.*, **157,** (1), 1–14. doi:10.1111/j.1365–246X.2004.02180.x.

Kayal, J.R., 1991. Earthquake prediction in Northeast India—a review, *Pure appl. Geophys.*, **136,** 297–313.

Kayal, J.R. 1998. Seismicity of North East and surrounding—development over the past 100 years, **29**(1), 31–67

Kayal, J.R., 2001. Microearthquake activity in some parts of the Himalaya and the tectonic model, *Tectonophysics*, **339,** 331–351.

Kayal, J.R. & Reena De, 1991. Microseismicitry and tectonics of northeast India, *BSSA*, **81**(1), 131–138.

Kayal, J.R., Gaonkar, S.G., Chakraborty, G.K. & Singh, O.P., 2004. Aftershocks and seismotectonics implications of the 13 September 2002 earthquake (M_w 6.5) in the Andaman Sea Basin, *Bull. seism. Soc. Am.*, **94**(**1**), 326–333.

Kayal, J.R. *et al*., 2006. Shillong plateau earthquakes in northeast India region: complex tectonic model, *Cur. Sci.*, **91,** 109–114.

Khan, P.K., 2005. Variation in dip-angle of the Indian plate subducting beneath the Burma plate and its tectonic implications, *Geosci. J.*, **9**(**3**), 227–234.

Khattri, K., Wyss, M., Gaur, V.K., Saha, S.N. & Bansal, V.K., 1983. Local seismic activity in the region of the Assam Gap, northeast India. *Bull. seism. Soc. Am.*, **73,** 459–470.

Le Dain A.Y., Tapponnier, P. & Molnar, P., 1984. Active faulting and tectonics of Burma and surrounding regions, *J. geophys. Res.*, **89,** 453–472.

Le Fort, P., 1975. Himalayas: the collided range. Present knowledge of the continental arc, *Am. J. Sci.*, **275A,** 1–44.

Lienert, B.R., Berg, B.E. & Frazer, L.N., 1986. Hypocenter: an earthquake location method using centered, scaled and adaptively damped least squares, *Bull. seism. Soc. Am.*, **76,** 771–783.

Mathur, L.P. & Evans, P., 1964. Oil in India, in *Proceedings of the 22nd Session of the International Geological Congress*, India, pp. 51–53.

Maung, H., 1987. Transcurrent movements in the Burma–Andaman Sea region, *Geology*, **15,** 911–912.

Q10

McKenzie, D. & Sclater, J.G., 1971. The evolution of the Indian Ocean since the late Cretaceous, *Geophys. J.R. astr. Soc.*, **25,** 437–528.

Mitchell, A.H.G., 1981. Phanerozoic plate boundaries in mainland SE Asia, the Himalaya and Tibet, *J. Geol. Soc. Lond.*, **138,** 109–122.

Mitchell, A.H.G. & McKerrow, W.S., 1975. Analoguous evolution of the Burma orogen and the Scottish Caledonides, *Geol. Soc. Am. Bull.*, **86,** 305–315.

Mitra, S., Priestley, K., Bhattacharyya, A. & Gaur, V.K., 2005. Crustal structure and earthquake focal depths beneath northeastern India and southern Tibet, *Geophys. J. Int.*, **160,** 227–248, doi:10.111 1/j.1365–246X.2004.02470.x.

Molnar, P. & Tapponnier, P., 1975. Cenozoic tectonics of Asia: effects of a continental collision, *Science*, **189,** 419–426.

Mukhopadhyay, M. & Dasgupta, S., 1988. Deep structure and tectonics of the Burmese arc: constraints from earthquake and gravity data, *Tectonophysics*, **149,** 299–322.

Murthy, M.V.N., Talukdar S.C. & Batthacharya, A.C., 1969. The Dauki Fault of Assam. *Bull. Oil Nat. Gas Comm.*, **6,** 57–64.

Nandy, D.R., 2001. *Geodynamics of Northeastern India and Adjoining Region*, ABC Publ., Kolkata, India, 209 pp.

Nandy, D.R. & Das Gupta, S., 1986. Application of remote sensing in Regional geological studies: a case study in Northeastern part of India. in *Proceedings of the International Seminar on* Photogrammetry and Remote Sensing for Developing Countries,Vol. 1, T.4-P/6, 1-t-P/6.4.

Ni, J.F., Guzman-Speziale, M., Bevis, M., Holt, W.E., Wallace, T.C. & Seager, W.R., 1989. Accretionary tectonics of Burma and the three-dimensional geometry of the Burma subduction zone, *Geology*, **17,** 68–71.

Okada, H., Suzuki, S., Asano, S., 1970. Anomalous underground structure in the Matsushiro earthquake swarm area as derived from a fan shooting technique, *Bull. Earthq. Res. Inst., Tokyo Univ.*, **48,** 811–833.

Oldham, R.D., 1899. Report on the great earthquake of 12th June, 1897, *Geol. Surv. Ind. Mem.*, **29,** 1–379.

Poddar, M.C., 1950. The Assam earthquake of 15th August, 1950, *Ind. Mineral.*, **4,** 167–176.

Rai, S.S., Srinagesh, D. & Srama, P.V.S.S.R, 1996. Morphology of the subducted Indian plate in the Indo–Burmese convergence zone, *Proc. Indian. Acad. Sci. (Earth Planet. Sci.)*, **105,** 441–450.

Rajendran, C.P., Rajendran, K., Duarah, B.P., Baruah, S. & Earnest, A., 2004. Interpreting the style of faulting and paleoseismicity associated with the 1897 Shillong, northeast India, earthquake: implications for regional tectonism, *Tectonics*, **23,** TC4009, doi:10.1029/2003 TC001605.

Rao, N.P. & Kumar, M.R., 1997. Uplift and tectonics of the Shillong plateau, northeast India, *J. Phys. Earth*, **45,** 167–176.

Rao, N.P., Kumar, M.R., 1999. Evidences for cessation of Indian plate subduction in the Burmese arc region, *Geophys. Res. Lett.*, **26,** 3149–3152.

Ravikumar, M., Purnachandra Rao, N., Chalam, S.V., 1996. A seismotectonic study of the Burma and Andaman arc regions using centroid moment tensor data, *Tectonophysics*, **253,** 155–165.

Satyabala, S.P., 1998. Subduction in the Indo–Burman region. Is it still active? *Geophys. Res. Lett.*, **25,** 3189–3192.

Socquet, A., Vigny, C., Chamot-Rooke, N., Simons, W., Rangin, C. & Ambrosius B., 2006. India and Sunda plates motion and deformation along their boundary in Myanmar determined by GPS. *J. geophys. Res.*, **111,** B05406, doi:10.1029/2005JB003877.

Tapponnier P., Pelzer G., Ledain A.Y., Armijo R. & Cobbold P., 1982. Propagating extrusion tectonics in Asia: new insights from simple experiments with plasticine, *Geology*, **10,** 611–616.

Tapponnier P., Peltzer G. & Armijo R., 1986. On the mechanics of the collision between India and Asia. in *Collision Tectonics*, *Geol. Soc. Spec. Publ.*,Vol. **9**, pp. 115–157, eds Coward, M.P., & Ries, A.C., Geol. Soc., London.

Thingbaijam, K.K. S., Nath S.K., Yadav, A., Raj, A., Walling Y. & Mohanty W.K., 2008. Recent seismicity in Northeast India and its adjoining region, *J. Seism.*, **12**:107–123, doi:10.1007/s10950–007–9074-y.

Tillottson, E., 1953. *The Great Assam Earthquake of 1950, the Completion of Papers on the Assam Earthquake of August 15, 1950*, Compiled by Ramchandra Rao M.B., pp.94–96.

Valdiya, K.S., 1980. Geology of Kumaun Lesser Himalaya. Debra Dun, India, *Stratigraphy and Correlations of Lesser Himalayan Formations*, eds Valdiya, K.S. & Bhatia, S.B., Hindustan Publishing Corporation, India, pp. 291.

Verma, R.K., Mukhopadhyay, M. & Ahluwalla, M.S., 1976, Earthquake mechanisms and tectonic features of northern Burma, *Tectonophysics*, **32,** 387–399.

Vigny, C. *et al*., 2003. Present-day crustal deformation around Sagaing fault, Myanmar, *J. geophys. Res.*, **108**(B11), 2533, doi:10.1029/2002JB001999.

Wallace, R.E., 1951. Geometry of shearing stress and relation to faulting, *J.Geol.*, **59,** 118–130.

Zhao, W., Nelson, K.D. & Project INDEPTH Team, 1993. Deep seismic reflection evidence for continental underthrusting beneath southern Tibet, *Nature*, **366,** 557–559.

Queries

Journal: GJI
Paper: gji_4107

Dear Author

During the copy-editing of your paper, the following queries arose. Please respond to these by marking up your proofs with the necessary changes/additions. Please write your answers on the query sheet if there is insufficient space on the page proofs. Please write clearly and follow the conventions shown on the corrections sheet. If returning the proof by fax do not write too close to the paper's edge. Please remember that illegible mark-ups may delay publication.

Query Reference	Query	Remarks
Q1	Author: Please check the term Iranges for correctness.	
Q2	Author: As per journal style only keywords from the keyword list are allowed. No other keywords are allowed so we have deleted the keywords. Please choose up to six key words from the attached list.	
Q3	Author: The inversion of focal . . .. . . from geodetic studies. This sentence has been reworded for clarity. Please check and confirm it is correct.	
Q4	Author: A running head short title was not supplied; please check if this one is suitable and, if not, please supply a short title of up to 45 characters (including space) that can be used instead.	
Q5	Author: Please check all the heading levels and numbers for correctness.	
Q6	Author: Das Gupta & Nandy 1992 has not been included in the Reference List, please supply full publication details.	
Q7	Author: Please check the term 'from 1997–2003 to 2006' for correctness.	
Q8	Author: Angelier & Bergerat 1987 has been changed to Angelier & Bergerat 1983 so that this citation matches the Reference List. Please confirm that this is correct.	
Q9	Author: Please check the term N0–30°E for correctness.	
Q10	Author: Please provide the publisher name and city location for Reference Mathur & Evans (1964).	
Q11	Author: Please check the style of Reference Nandy & Das Gupta for correctness.	
Q12	Author: Please provide the publisher name and city location for Reference Tillottson (1953).	

Key words

Authors are requested to choose key words from the list below to describe their work. The key words will be printed underneath the summary and are useful for readers and researchers. Key words should be separated by a semi-colon and listed in the order that they appear in this list. An article should contain no more than six key words.

GEOPHYSICAL METHODS
Time series analysis
Image processing
Neural networks, fuzzy logic
Numerical solutions
Fourier analysis
Wavelet transform
Instability analysis
Inverse theory
Numerical approximations and analysis
Persistence, memory, correlations, clustering
Probabilistic forecasting
Spatial analysis
Downhole methods
Tomography
Interferometry
Thermobarometry
Fractals and multifractals
Non-linear differential equations
Probability distributions
Self-organization

GEODESY and GRAVITY
Satellite geodesy
Reference systems
Sea level change
Space geodetic surveys
Seismic cycle
Transient deformation
Gravity anomalies and Earth structure
Geopotential theory
Time variable gravity
Earth rotation variations
Global change from geodesy
Lunar and planetary geodesy and gravity
Radar interferometry
Plate motions
Tides and planetary waves
Acoustic-gravity waves

GEOMAGNETISM and ELECTROMAGNETISM
Electrical properties
Electromagnetic theory
Magnetotelluric
Non-linear electromagnetics
Archaeomagnetism
Biogenic magnetic minerals
Dynamo: theories and simulations
Environmental magnetism
Geomagnetic excursions
Geomagnetic induction
Magnetic anomalies: modelling and interpretation
Magnetic and electrical properties
Magnetic fabrics and anisotropy
Magnetic mineralogy and petrology
Magnetostratigraphy
Palaeointensity
Palaeomagnetic secular variation
Palaeomagnetism applied to tectonics
Palaeomagnetism applied to geologic processes
Rapid time variations
Remagnetization
Reversals: process, timescale, magnetostratigraphy
Rock and mineral magnetism
Satellite magnetics
Marine magnetics and palaeomagnetics
Marine electromagnetics

GENERAL SUBJECTS
Geomorphology
Geomechanics
Glaciology
Hydrogeophysics
Ionosphere/atmosphere interactions
Ionosphere/magnetosphere interactions
Gas and hydrate systems
Ocean drilling
Hydrology
Ultra-high pressure metamorphism
Ultra-high temperature metamorphism
Tsunamis
Thermochronology
Heat flow
Hydrothermal systems
Mantle processes

COMPOSITION and PHYSICAL PROPERTIES
Microstructure
Permeability and porosity
Plasticity, diffusion, and creep
Composition of the core
Composition of the continental crust
Composition of the oceanic crust
Composition of the mantle
Composition of the planets
Creep and deformation
Defects
Elasticity and anelasticity
Equations of state
High-pressure behaviour
Fracture and flow
Friction
Fault zone rheology
Phase transitions

SEISMOLOGY
Controlled source seismology
Earthquake dynamics
Earthquake ground motions
Earthquake source observations
Seismic monitoring and test-ban treaty verification
Palaeoseismology
Earthquake interaction, forecasting, and prediction
Seismicity and tectonics
Body waves
Surface waves and free oscillations
Interface waves
Guided waves
Seismic anisotropy
Seismic attenuation
Site effects
Seismic tomography
Volcano seismology
Computational seismology
Theoretical seismology
Statistical seismology
Wave scattering and diffraction
Wave propagation
Acoustic properties
Early warning
Rheology and friction of fault zones

TECTONOPHYSICS
Planetary tectonics
Mid-ocean ridge processes
Transform faults
Subduction zone processes
Intra-plate processes
Volcanic arc processes
Back-arc basin processes
Cratons
Continental margins: convergent
Continental margins: divergent
Continental margins: transform
Continental neotectonics
Continental tectonics: compressional
Continental tectonics: extensional
Continental tectonics: strike-slip and transform
Sedimentary basin processes
Oceanic hotspots and intraplate volcanism
Oceanic plateaus and microcontinents
Oceanic transform and fracture zone processes
Submarine landslides
Submarine tectonics and volcanism
Tectonics and landscape evolution
Tectonics and climatic interactions
Dynamics and mechanics of faulting
Dynamics of lithosphere and mantle
Dynamics: convection currents, and mantle plumes
Dynamics: gravity and tectonics
Dynamics: seismotectonics
Heat generation and transport
Impact phenomena
Hotspots
Large igneous provinces
Lithospheric flexure

Obduction tectonics
Neotectonics
Diapir and diapirism
Dynamics and mechanics of faulting
Folds and folding
Fractures and faults
Kinematics of crustal and mantle deformation
High strain deformation zones
Crustal structure
Mechanics, theory, and modelling
Microstructures
Rheology: crust and lithosphere
Rheology: mantle
Rheology and friction of fault zones
Paleoseismology

PLANETS
Planetary interiors
Planetary volcanism

VOLCANOLOGY
Physics of magma and magma bodies
Magma chamber processes
Magma genesis and partial melting
Pluton emplacement
Effusive volcanism
Mud volcanism
Subaqueous volcanism
Explosive volcanism
Planetary volcanism
Volcaniclastic deposits
Volcano/climate interactions
Atmospheric effects (volcano)
Volcanic gases
Lava rheology and morphology
Magma migration and fragmentation
Eruption mechanisms and flow emplacement
Physics and chemistry of magma bodies
Calderas
Experimental volcanism
Tephrochronology
Remote sensing of volcanoes
Volcano monitoring
Volcanic hazards and risks
Volcano seismology

GEOGRAPHIC LOCATION
Africa
Antarctica
Arctic region
Asia
Atlantic Ocean
Australia
Europe
Indian Ocean
North America
Pacific Ocean
South America

MARKED PROOF

Please correct and return this set

Please use the proof correction marks shown below for all alterations and corrections. If you wish to return your proof by fax you should ensure that all amendments are written clearly in dark ink and are made well within the page margins.

Instruction to printer	*Textual mark*	*Marginal mark*
Leave unchanged	··· under matter to remain	✓
Insert in text the matter indicated in the margin		New matter followed by or
Delete	/ through single character, rule or underline or ⊢⊣ through all characters to be deleted	 or
Substitute character or substitute part of one or more word(s)	/ through letter or ⊢⊣ through characters	new character / or new characters /
Change to italics	— under matter to be changed	
Change to capitals	≡ under matter to be changed	≡
Change to small capitals	≡ under matter to be changed	≡
Change to bold type	~ under matter to be changed	~
Change to bold italic	~ under matter to be changed	
Change to lower case	Encircle matter to be changed	
Change italic to upright type	(As above)	
Change bold to non-bold type	(As above)	
Insert 'superior' character	/ through character or where required	 or under character e.g. or
Insert 'inferior' character	(As above)	 over character e.g.
Insert full stop	(As above)	⊙
Insert comma	(As above)	,
Insert single quotation marks	(As above)	 or and/or or
Insert double quotation marks	(As above)	 or and/or or
Insert hyphen	(As above)	⊢
Start new paragraph		
No new paragraph		
Transpose		
Close up	linking ⌒ characters	⌒
Insert or substitute space between characters or words	/ through character or where required	
Reduce space between characters or words	between characters or words affected